



BACCHUS

Impact of Biogenic versus Anthropogenic emissions on Clouds and Climate: towards a Holistic UnderStanding

Collaborative Project

SEVENTH FRAMEWORK PROGRAMME
ENV.2013.6.1-2

Atmospheric processes, eco-systems and climate change

Grant agreement no: 603445

Deliverable number:	D3.4
Deliverable name:	Evaluation of global ESMs and connection of regional case studies through global modelling, satellite data and global compilations of in-situ data
WP number:	3
Delivery date:	Project month 43 (30/06/2017)
Actual date of submission:	30/06/2017
Dissemination level:	PU
Lead beneficiary:	FMI
Responsible scientist/administrator:	Giulia Saponaro
Estimated effort (PM):	33.95
Contributor(s):	Katty Huang (ETHZ), Inger Helene H. Karset (UIO), Harri Kokkola (FMI), Pekka Kolmonen (FMI), David Neubauer (ETHZ), Giulia Saponaro (FMI), Larisa Sogacheva (FMI), Moa Sporre (UIO)

Estimated effort contributor(s) (PM):	FMI: 26.25 PM (0.37 not charged to BACCHUS); ETHZ: 6.7 PM (0.7 PM not charged to BACCHUS); UIO: 1 PM (0.37 PM not charged to BACCHUS)
Internal reviewer:	Philip Stier

1. Objectives and executive summary

This deliverable aimed at the evaluation of aerosol and cloud properties obtained from three different Earth System Models (ECHAM6-HAM, ECHAM6-HAM-SALSA and NorESM) and satellite data, with the final goal of understanding how to improve the ESMs to investigate aerosol and cloud interaction on both global and regional scales.

For this purpose, the ESMs were set up for a hindcast over 2008 with the meteorology nudged to ECMWF data to collect direct aerosol and cloud properties and, additionally, the module MODIS-COSP (version 1.4 for ECHAM6-HAM, ECHAM6-HAM-SALSA whilst version 1.3 for NorESM) was applied to obtain MODIS-like cloud diagnostics. Collection 6 MODIS Level 3 daily data were used for evaluation on the global scale, while ADV AATSR data was used to connect the evaluation with the Amazon case study, one of the regions selected in the framework of the BACCHUS project and also investigated in support of Task 3.3.

NorESM shows reasonable results compared to the other models except from the cases of cloud effective radius for ice clouds and IWP. In the used version of COSP, snow (snow particle size and snow optical thickness) are included in the calculations of cloud effective radius (CER) and optical thickness (COT) for ice clouds. Therefore, since IWP is calculated from CER and COT in ice cloud, the snow also affects IWP. ECHAM6-HAM and ECHAM6-HAM-SALSA have diagnostic precipitation and snow is not included in the calculation of IWP or COT. In the code of COSPv1.4 implementation, the cloud effective radius and optical thickness of ice clouds are computed only from IWP and ICNC. Therefore the addition of snow could explain the higher values of CER for ice clouds and IWP in NorESM. The comparison of ECHAM-HAM2 and ECHAM-HAM2-SALSA is interesting because they only differ in the representation of the aerosol size distribution. For example, LWP and CER for liquid clouds are quite different between these two model versions. However, ice related variables seem to be generally much closer. The large differences in the liquid clouds between ECHAM6-HAM and ECHAM6-HAM-SALSA are related to the different tuning between ECHAM6-HAM and ECHAM6-HAM-SALSA: in particular the minimum CDNC concentration and the auto-conversion rate tuning parameters were different.

The outcome of the combined WP3 and WP4 workshop during BACCHUS AM 2017 was the additional task of constraining the ICNC to possibly improve the simulation of mixed phase

clouds. The work is still on going and we will be attempting to publish the outcome in a peer-reviewed journal.

2. Data

2.1. Satellite

2.1.1. MODIS

We used regular gridded Level 3 daily data acquired from the MODIS instruments (Aqua and Terra) for the year 2008. Global aerosol optical depth (AOD) is derived at 550nm while other parameters accounting for the particle size distribution (such as the Ångström exponent or fine-mode aerosol optical depth) are derived either over land or over ocean (Levy et al., 2013).

Unlike in the previous datasets, in Collection 6, which is used in this work, the provided cloud optical parameters are divided into different products accordingly to the cloud phase and retrieved, additionally to the nominal 2.1 μm , at 1.6 μm and 3.7 μm . In this study we used the cloud properties at 2.1 μm for ice and liquid clouds (Hubanks et al, 2016). Moreover, we derive the cloud droplet number concentration from the retrieved cloud effective radius and optical thickness following the method presented in Brenguier et al. (2000) that is valid under the assumption of adiabatic clouds

2.1.2. ADV AATSR

The ATSR dual view (ADV, over land) and single view (ASV, over ocean) algorithms (Kolmonen et al, 2016; Sogacheva et al., 2017) have been developed at the FMI to derive aerosol properties from the AATSR radiances over land and over ocean respectively, while the newly implemented cloud module SACURA in the ADV/ASV algorithm retrieves cloud properties. The results are valuable as an inter-comparison resource for the MODIS aerosol and cloud products, and, since the ATSR algorithms can be run internally at FMI in the nominal 1x1 km resolution, aerosol-cloud boundaries can be studied. We used the aggregated L3 at 1 x1 degree resolution for comparison with MODIS and models data.

2.2. ESM

2.2.1. ECHAM6-HAM

ECHAM-HAMMOZ (echam6.3-ham2.3-moz1.0) is a global aerosol-chemistry climate model. Only the global aerosol-climate model part of ECHAM-HAMMOZ is used here and referred to as ECHAM6-HAM (Lohmann et al., in prep.). It consists of the general circulation model ECHAM6 (Stevens et al., 2013) coupled to the latest version of the aerosol module HAM2 (Zhang et al., 2012) and uses a two-moment cloud microphysics scheme that includes prognostic equations for the cloud droplet and ice crystal number concentrations as well as cloud water and cloud ice (Lohmann et al., 2007; Lohmann and Hoose, 2009). The stratiform cloud scheme consists of prognostic equations for the water phases (vapor, liquid, solid), bulk cloud microphysics (see above), and an empirical cloud cover scheme (Sundqvist et al., 1989). The ice crystal cirrus scheme is based on Kärcher and Lohmann (2002) and described in Lohmann et al. (2008). The autoconversion of cloud droplets to rain follows Khairoutdinov and Kogan (2000). Immersion and contact freezing follows Lohmann and Diehl (2006). Cumulus convection is represented by the parameterization of Tiedtke (1989) with modifications by Nordeng (1994) for deep convection.

Simulations were performed at T63 ($1.9^\circ \times 1.9^\circ$) spectral resolution using 31 vertical levels (L31) and COSP v1.4. Horizontal winds and surface pressure were nudged towards the ERA-Interim (Dee et al., 2011) reanalysis for 2008 and observed sea surface temperatures and sea ice cover for 2008 were used (<http://www-pcmdi.llnl.gov/projects/amip/>). 3 hourly instantaneous output was used (the COSP output is almost instantaneous as it is the 3 hour average over 2 hour time steps i.e. 50% of the values are instantaneous and the other 50 % are an average over two time steps).

2.2.2. ECHAM6-HAM-SALSA

ECHAM-HAMMOZ-SALSA is identical to the ECHAM-HAMMOZ setup (echam6.3-ham2.3-moz1.0), with the difference that the sectional aerosol module SALSA (Kokkola et al., 2008) is used instead of the modal model M7 used in ECHAM6-HAM setup. SALSA calculates the aerosol microphysical processes: nucleation, coagulation, condensation, and hydration. In this setup, the aerosol model HAM applies also the sectional scheme for the rest of the aerosol processes, i.e. emissions, removal, radiative effects, and aerosol-cloud interactions. The

implementation and the evaluation of SALSA to ECHAM-HAMMOZ has been presented by Bergman et al. (2012) and its latest modifications by Laakso et al. (2016).

Similarly to ECHAM6-HAM, simulations were performed at T63 ($1.9^\circ \times 1.9^\circ$) spectral resolution using 31 vertical levels (L31) and COSP v1.4. Horizontal winds and surface pressure were nudged towards the ERA-Interim (Dee et al., 2011) reanalysis for 2008 and observed sea surface temperatures and sea ice cover for 2008 were used (<http://www-pcmdi.llnl.gov/projects/amip/>). The 3-hourly instantaneous output was used.

2.2.3. NorESM

The Norwegian Earth System Model (NorESM) (Bentsen et al., 2013) is largely based on the CESM model but uses a different ocean model (MICOM) and a different aerosol scheme in the atmospheric model CAM. The aerosol scheme in the NorESM version of CAM, called CAM-Oslo, can be described as an aerosol life cycle scheme which calculates production tagged mass concentrations of different aerosol species (Kirkevåg et al., 2013). In the current simulations the NorESM model was run with the CAM-Oslo version 5.3 (Kirkevåg et al., 2017) which is configured with the microphysical two moment scheme MG1.5 (Morrison and Gettelman, 2008; Gettelman and Morrison, 2015) for stratiform clouds. The scheme includes prognostic equations for liquid (mass and number) and ice (mass and number) and a version of the Khairoutdinov and Kogan (2000) autoconversion scheme where subgrid variability of cloud water (Morrison and Gettelman, 2008) has been included. The aerosol activation follows the Liu et al. (2012) method including the simplifications put forward by Ghan and Easter (2006). The heterogeneous freezing in CAM5.3-Oslo is based on Wang et al. (2014) with a correction applied to the contact angle model (Kirkevåg et al., 2017). Moreover, CAM5.3-Oslo has a shallow convection scheme (Park and Bretherton, 2009) and a deep convection scheme (Zhang and McFarlane, 1995).

The simulation was run with the Community land model (CLM) version 4.5 (Oleson et al., 2010) with satellite phenology. Included in CLM is the Model of Emissions of Gases and Aerosols from Nature (MEGAN) version 2.1. (Guenther et al., 2012) which interactively calculates the emissions of biogenic volatile organic vapors. Both isoprene and monoterpenes take part in formation of secondary organic aerosol in CAM5.3-Oslo. The sea surface temperatures and sea ice in the simulation were prescribed monthly averages for the years 1982-2001. The resolution

for the simulation was $0.9 \times 1.25^\circ$ and the surface pressures as well as horizontal winds were nudged against ERA-Interim reanalysis data (Berrisford et al., 2011) from 2008. CAM-Oslo was run with COSP version 1.3 producing 3 hourly instantaneous outputs.

3. Methods

Prior to their inter-comparison the ESM and satellite data were collocated both in time and space. The model 3-h outputs were aggregated to daily averages and successively re-gridded onto the finer satellite regular grid of $1^\circ \times 1^\circ$ by linear interpolation. The evaluation and statistical analysis were performed on resulting datasets passing the criteria of pixel-level collocation across all datasets. As MODIS L3 daily data provide grid values for in-cloud pixels only (and clear sky only for AOD), ESMs output data were also derived for in-cloud pixels only by dividing the averaged-grid values by their corresponding cloud fractions. We compare COSP-derived modelling variables (cloud fraction, effective radius and water contents) and direct ones (CDNC and AOD) with MODIS retrieval (see Appendix B).

4. Results

The content of the deliverable addresses the global evaluation between ESMs and satellite data in the following order:

- Distribution of the observations
- Spatial distribution of the difference between MODIS and modelling observations
- Scatter plots
- Cloud effective radius (CER)-, cloud fraction (CF)-, cloud water path (CWP)- AOD relationships

Histograms

Aiming to understand the possible discrepancies between satellite and modelling observation, histograms provide an insight of data frequency distribution. For each parameter, its frequency distribution is computed, where the bin width is determined by 1% of the maximum value, and the obtained number of observations per bin is divided by the total number of points resulting into the fraction of observations. The analysis is iterated globally and over geographical regions defined in Myhre et al. (2007) and shown in Fig.1.

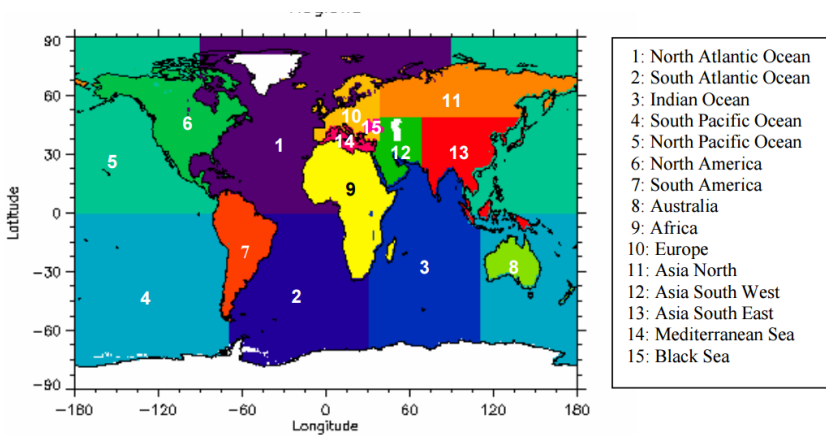


Figure 1. Geographical region applied in the analysis. Figure borrowed from Myhre et al. (2007).

Global scale

Figure 2 shows that the peak of MODIS and ECHAM6-HAM-SALSA data, respectively, are centered on 0.07 while ECHAM6-HAM and NorESM AOD frequency distribution peaks are shifted towards AOD values smaller than 0.05.

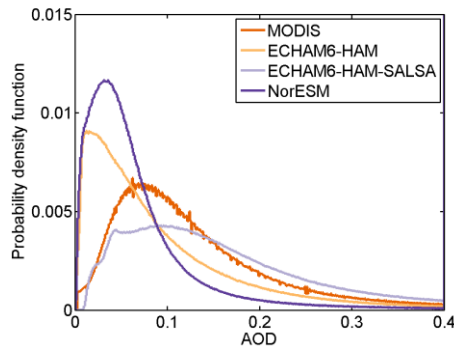


Figure 2. Fraction of AOD observations at 550 nm for the four datasets.

The cloud fraction distributions show similar patterns for ice clouds (Fig.3b) and the liquid cloud fraction (Fig.3c): unlike MODIS, none of the models provides outputs for low amounts of CF and their distribution is monotonically increasing with a peak up of 8% for CF =1. MODIS detects around 4% of CF near 0 for both ice and liquid cloud CF. In the case of liquid water clouds (Fig.3c), the 4 datasets have similar frequency distributions in the range of 0.4-0.6, while differences are large over the extremes. MODIS detects almost 4% of the pixel to be nearly cloud-free, NorESM evaluates 2% of the pixels to have a CF below 0.2, and both ECHAM6-

HAM and ECHAM6-HAM-SALSA shows negligible amount of CF below 0.2. Pincus et al. (2012) shows that cloud fraction is quite sensitive to the spatial scale at which it is measured and that MODIS Collection 5 has 15% less total cloud cover than ISCCP because of the different treatment of partly covered pixels. This could be one reason explaining the differences between models and MODIS cloud fraction.

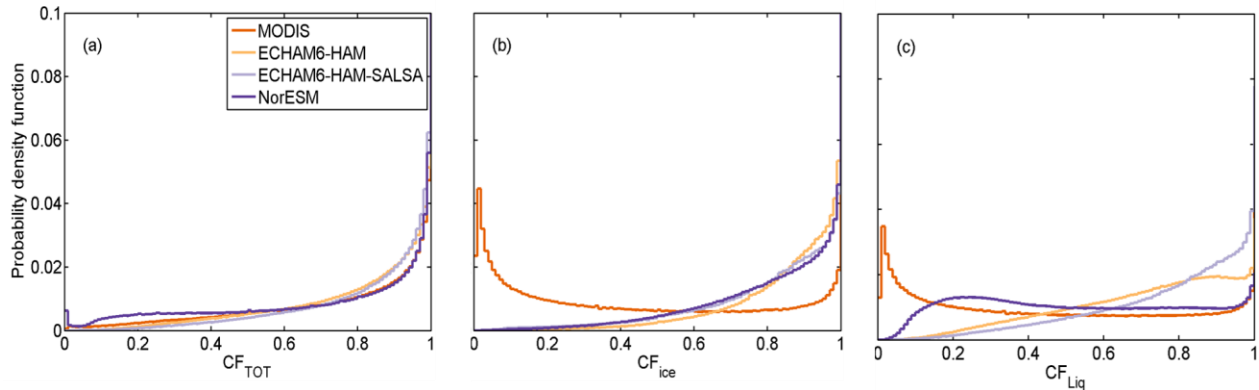


Figure 3. Fraction of CF observations for the four datasets for three cases: total (combined ice and liquid) cloud fraction (a), ice-phase clouds (b), and liquid-phase clouds (c).

Figure 4 shows the results inherent to the IWP (Fig.4a) and LWP (Fig.4b) and CER for ice-clouds (Fig.4c) and liquid water clouds (Fig.4d).

IWP (Fig.4a) has a very similar distribution for the results obtained from MODIS, ECHAM6-HAM and ECHAM6-HAM-SALSA where most of the distribution is found for IWP < 200 gm^{-2} and less than 0.05% for IWP > 1000 gm^{-2} . NorESM shows IWP values up to 3000 gm^{-2} (not shown in the picture). For LWP the agreement between MODIS and the models is better with the main difference that ECHAM6-HAM has nearly 10% of data centered around 100 gm^{-2} (Fig.4b). The results of CER for liquid water clouds (Fig.4c) show that the distributions are centered on 10 μm , with the lower bounds around 5 μm . The upper bounds of the distribution are quite different: while less than 10% of data are retrieved for CER > 14 μm , 17 μm , 20 μm and 25 μm for ECHAM-HAM, NorESM, ECHAM-HAM-SALSA and MODIS respectively. For ice clouds MODIS, ECHAM6-HAM, and ECHAM6-HAM-SALSA have similar width for 60% of the data, although the distribution are centered on 25 μm for ECHAM6-HAM and ECHAM6-HAM-SALSA while around 30 μm for MODIS. NorESM CER is wider distributed and shifted towards higher CER values. Further investigations are needed to understand why CER for ice clouds are biased towards higher values in NorESM.

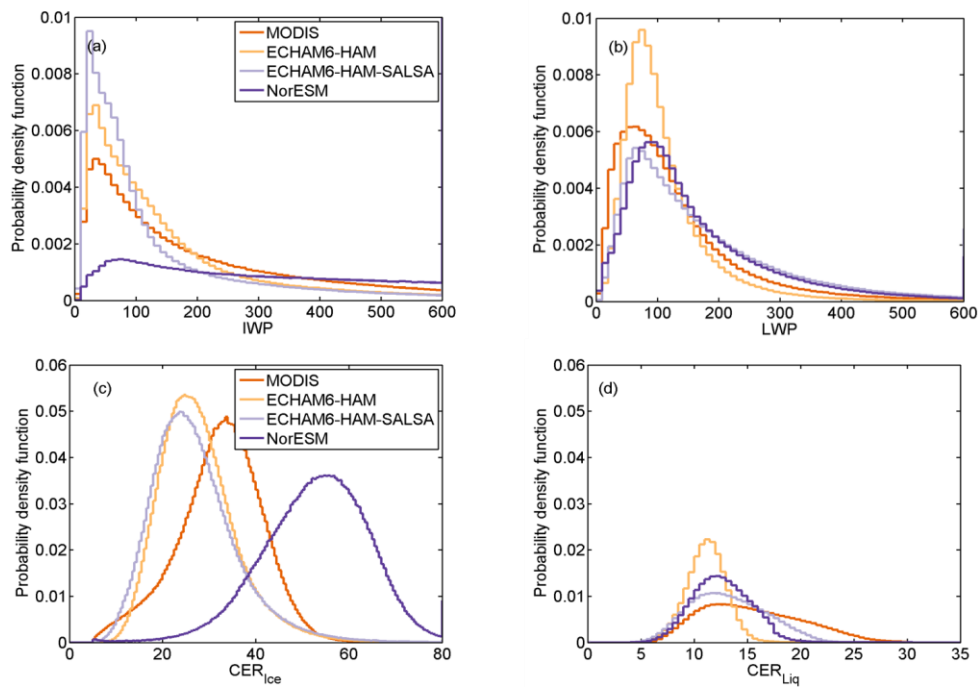


Figure 4. Fraction of observation for CWP and CER for ice-phase clouds (a, c) and water-phase clouds (b, d)

Regional scale

The probability density functions for the parameters introduced in the previous section are now iterated for the different geographical regions illustrated in Fig.1.

Overall, there are not large differences between the global PDF and the regional ones and within the regional analysis there is a reasonable agreement.

Figure 5 shows that AOD pdfs varies quite significantly from region to region: over the oceans the PDFs patterns are similar to each other's. Over North America (Fig.5f,j,k), Europe and Northern Asia ECHAM6-HAM has a peak for very low AOD, which is absent in the other region and from the other data sources. Perhaps this can be explained by high rainout/washout rates in the Mid-Latitude frontal systems. Moreover, the presence of low values in ECHAM6-HAM but not ECHAM6-HAM-SALSA could be caused by the different tuning as well as by the different representation of the aerosol size distribution.

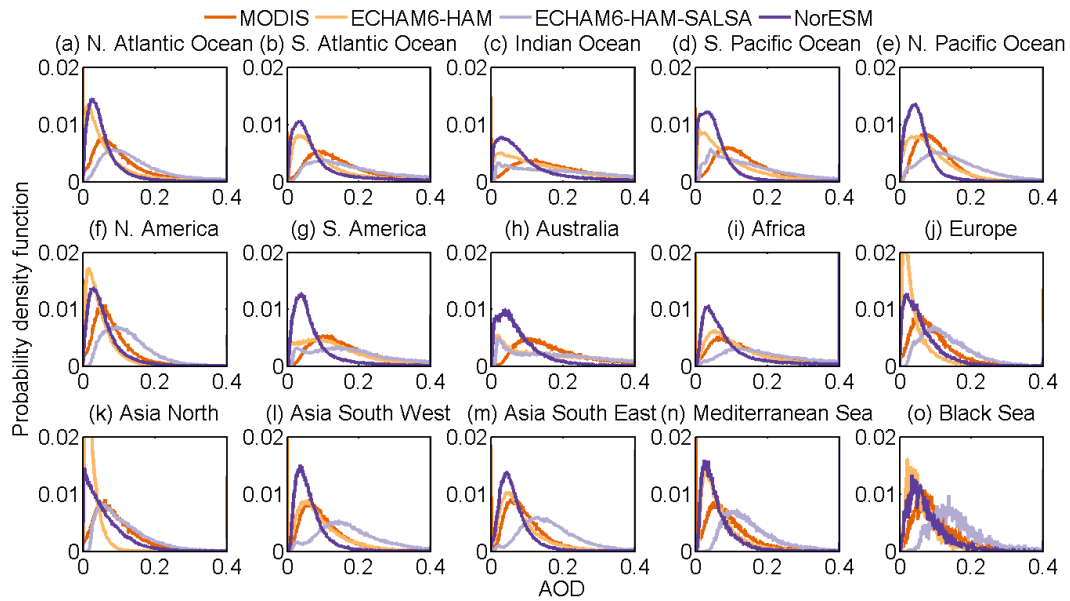


Figure 5. AOD (550nm) probability distribution for the four data sources (MODIS, ECHAM6-HAM, ECHAM6-HAM-SALSA, NorESM) sub-divided by regions shown in Fig.1.

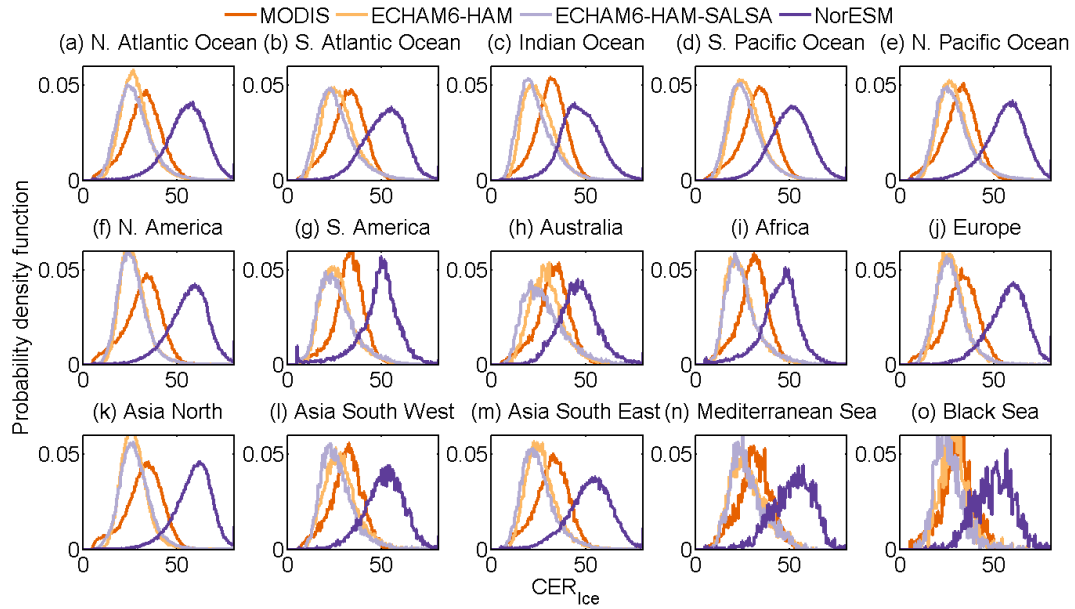


Figure 6. CER for ice clouds probability distribution for the four data sources (MODIS, ECHAM6-HAM, ECHAM6-HAM-SALSA, NorESM) sub-divided by regions shown in Fig.1.

The cloud effective radius (Fig.7) for liquid clouds shows that ECHAM6-HAM and ECHAM6-HAM-SALSA have similar PDFs through the regions, MODIS and NorESM present different distributions: MODIS peak shifts from 15 μ m as seen in Fig.4d to 22 μ m over the region of South America (Fig.7g), while NorESM presents a second peak over the region of Europe (Fig.7j), Mediterranean Sea (Fig.7n).

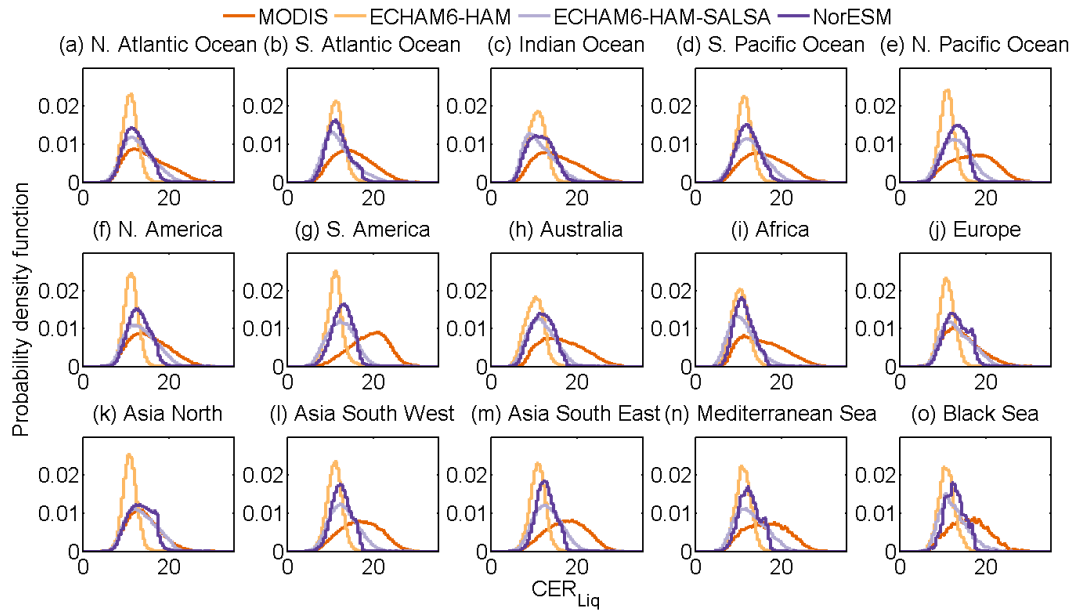


Figure 7. Liquid CER probability distribution for the four data sources (MODIS, ECHAM6-HAM, ECHAM6-HAM-SALSA, NorESM) sub-divided by regions shown in Fig.1.

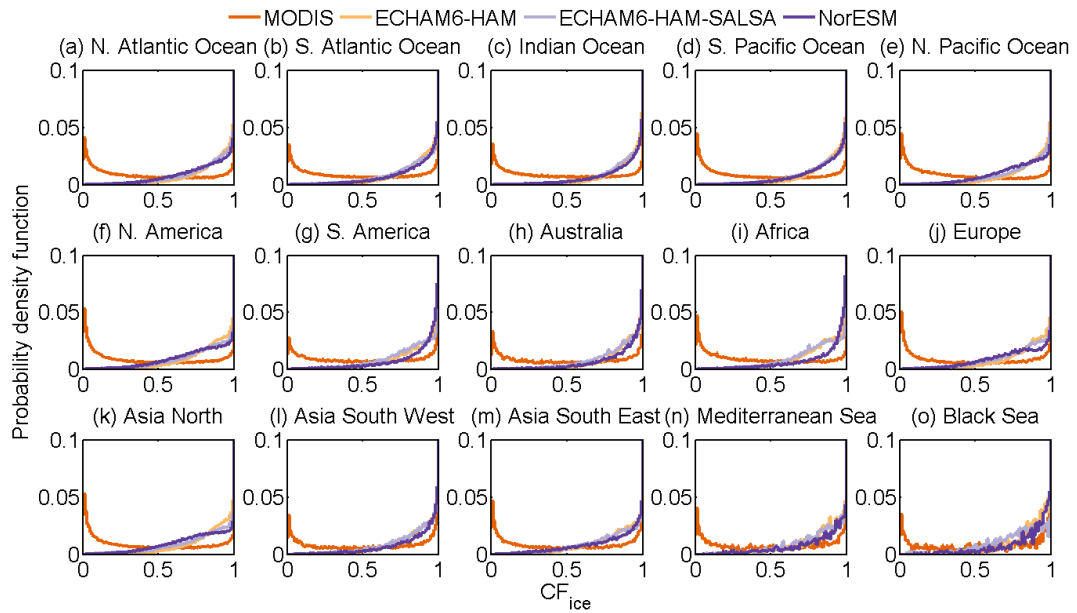


Figure 8. CF for ice cloud probability distribution for the four data sources (MODIS, ECHAM6-HAM, ECHAM6-HAM-SALSA, NorESM) sub-divided by regions shown in Fig.1.

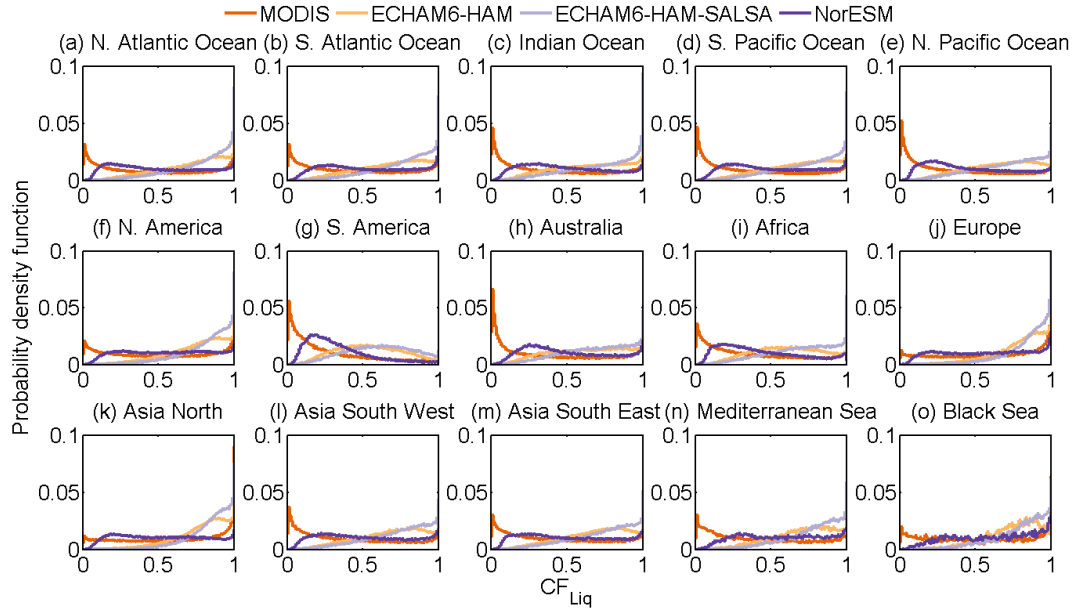


Figure 9. CF for liquid cloud probability distribution for the four data sources (MODIS, ECHAM6-HAM, ECHAM6-HAM-SALSA, NorESM) sub-divided by regions shown in Fig.1.

Unlike the models, MODIS retrieves up 5% of data for very low CF. MODIS and NorESM have the same distributions for $CF > 0.1$. Over South America (Fig.9g) none of the data source show values for $CF = 1$.

One possible explanation about the discrepancy between CF_{Ice} and CF_{Liq} may be found in the new definition of MODIS ‘*Cloud_Fraction_Ice*’ and ‘*Cloud Fraction Liquid*’ presented in Collection 6. While in the models and in the previous MODIS Collection 5/51, the ‘*Cloud Optical Properties Cloud Fraction*’ was defined only by clear pixels and successfully retrieved pixels in the computation of the denominator, the most recent Collection 6 uses clear pixels, successfully retrieved pixels, and unsuccessfully retrieved pixels in the computation of the denominator, which effectively causes a slight reduction in the computed cloud fractions between C5/51 and C6.

These two parameters are now defined by the ratio between the number of successful and unsuccessful liquid water (/ice) cloud retrievals and the sum of clear, successful and unsuccessful retrievals for all phases (Husbank et al., 2016). Therefore, lower values for these parameters are expected when comparing with Collection 5 data and possibly with modelling data. From both global and regional distribution it can be observed the MODIS is the only data source retrieving up 5% of data for very low CF, while for $CF = 1$ show the lowest amount of data.

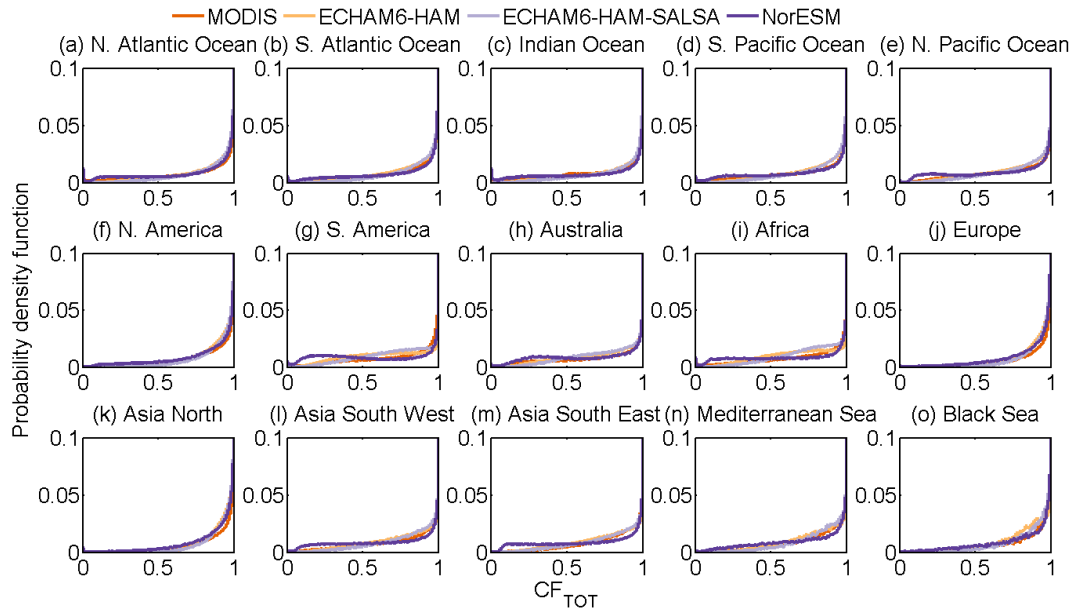


Figure 10. Total CF probability distribution for the four data sources (MODIS, ECHAM6-HAM, ECHAM6-HAM-SALSA, NorESM) sub-divided by regions shown in Fig.1.

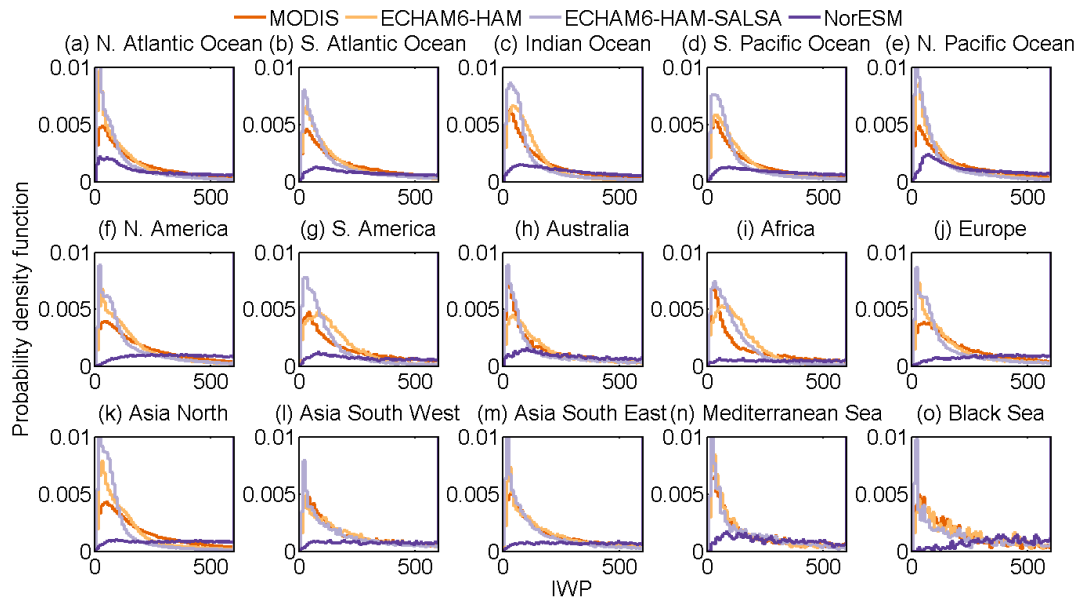


Figure 11. IWP probability distribution for the four data sources (MODIS, ECHAM6-HAM, ECHAM6-HAM-SALSA, NorESM) sub-divided by regions shown in Fig.1.

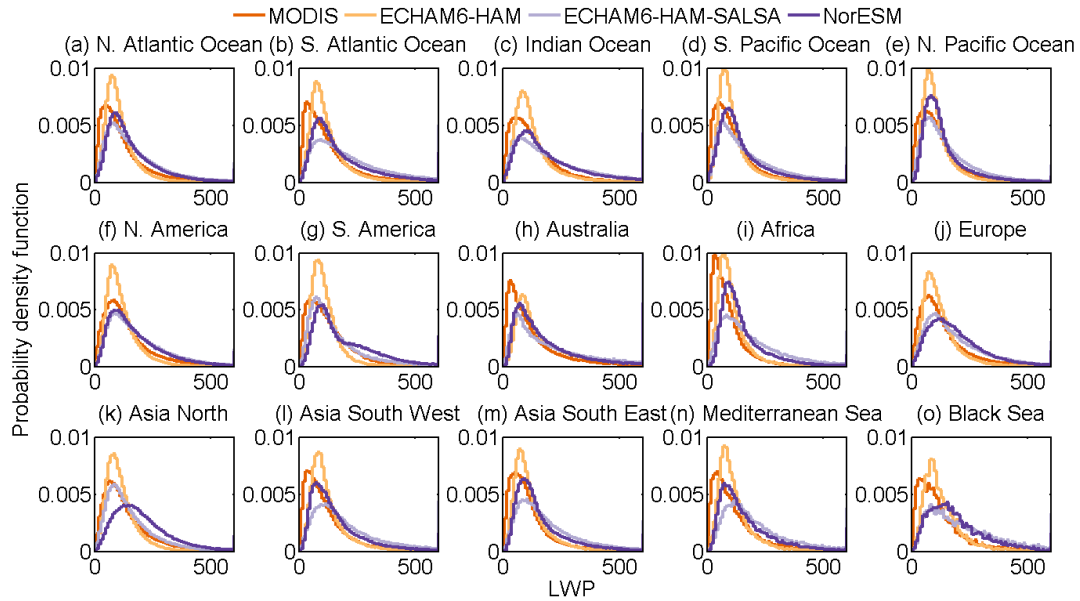


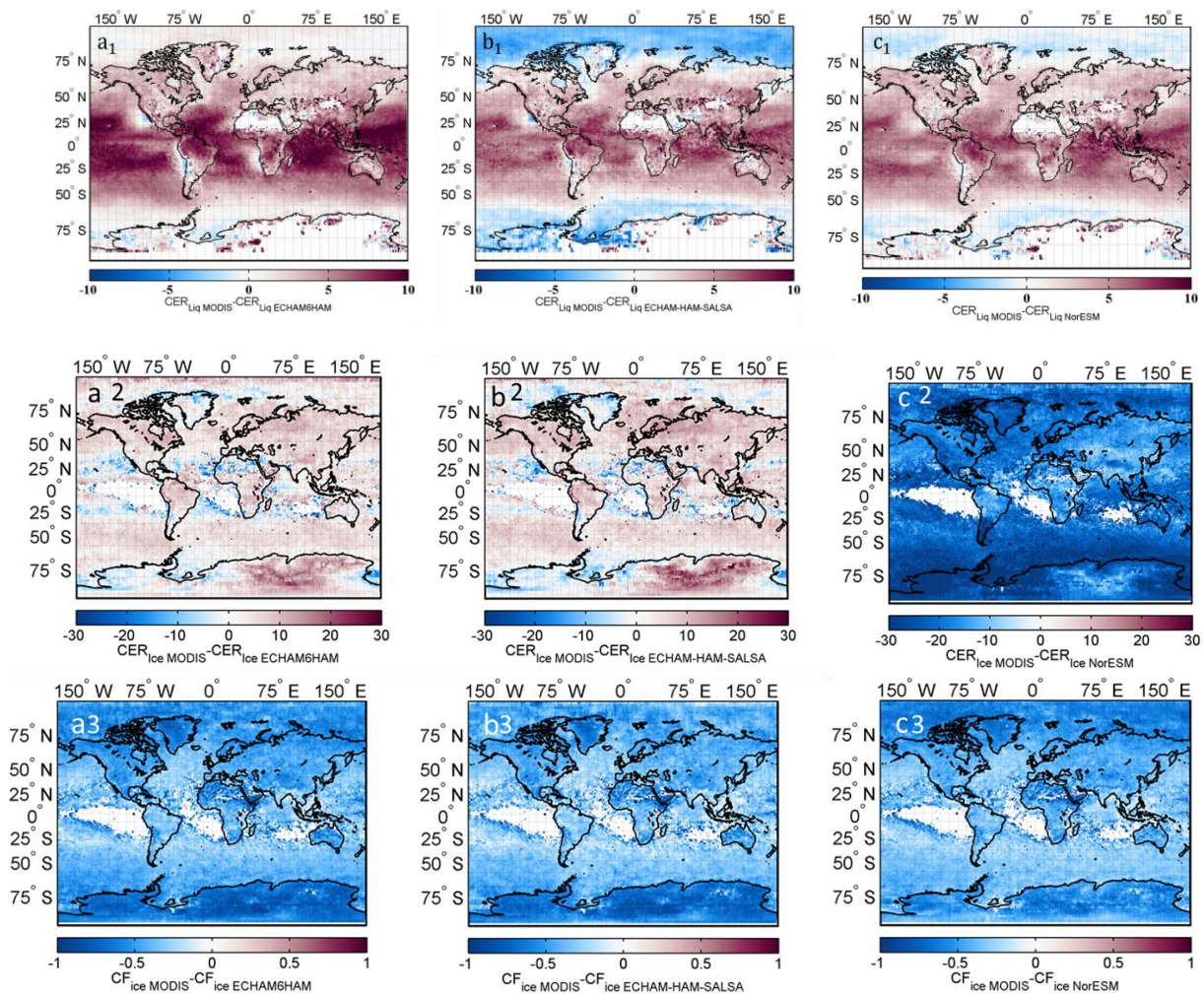
Figure 12. LWP probability distribution for the four data sources (MODIS, ECHAM6-HAM, ECHAM6-HAM-SALSA, NorESM) sub-divided by regions shown in Fig.1.

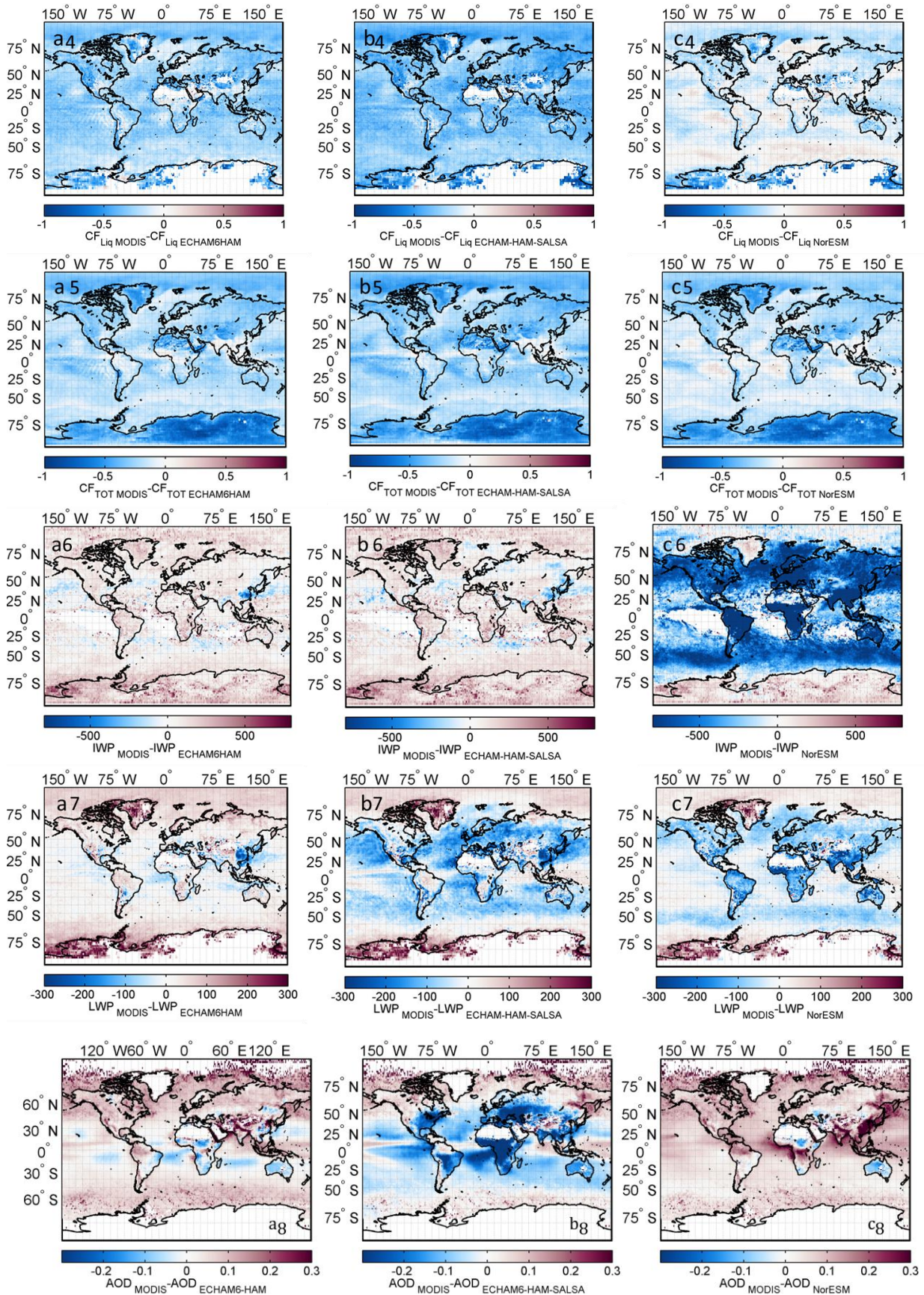
Spatial distribution of the difference between MODIS and modelling observations

The differences between the dataset are now shown as spatial distribution.

At mid-latitudes MODIS estimates of CER are higher than the models values (Fig.13.1). Over the poles good agreement is found between MODIS and ECHAM6-HAM (Fig.13.a1) and NorESM (Fig.13.c1) while ECHAM6-HAM-SALSA overestimates the CER value over the Polar Regions (Fig.13.b1). For ice-cloud cases, large discrepancies of NorESM from the other models and MODIS were already found in the previous sections for CER and IWP, with the former having large bias towards high values; this result is confirmed in Fig.13.c2 and Fig.13.c6, where the figures show a global negative difference. Additionally, the IWP is positive only over Antarctica and Greenland. In the comparisons of CER and IWP with the other two models, shown in Fig.13.a2, b2 and Fig.13.a6 and b6, the results are very similar to each other with differences ranging both from positive to negative values. Figure 13.7 shows the spatial distribution of LWP: while over the polar region MODIS observations are higher, at mid-latitudes the difference between MODIS and ECHAM6-HAM-SALSA and NorESM is negative, while MODIS and ECHAM6-HAM show better agreement. Only for liquid water clouds, MODIS and NorESM cloud fraction are in good agreement for most areas over the globe. In fact their distributions are

very similar for $CF > 0.2$ (Fig.3c). ECHAM6-HAM-SALSA AOD (Fig.13.8b) shows significant biases over mid-latitudes when compared with the results of the other two models (Fig.13.8a,c). MODIS shows unreliable CDNC around the poles as a consequence of the retrievals of large CER over these areas. This results in the high overestimates differences for all considered cases. Focusing in the range of $\pm 60^\circ$ Latitude, the larger discrepancies are between MODIS and NorESM (Fig.13.9c) with the latter strongly overestimating over oceans. ECHAM6-HAM and ECHAM6-HAM-SALSA (Fig.13.8a,b) show rather an overestimation of the models over ocean and underestimation over land.





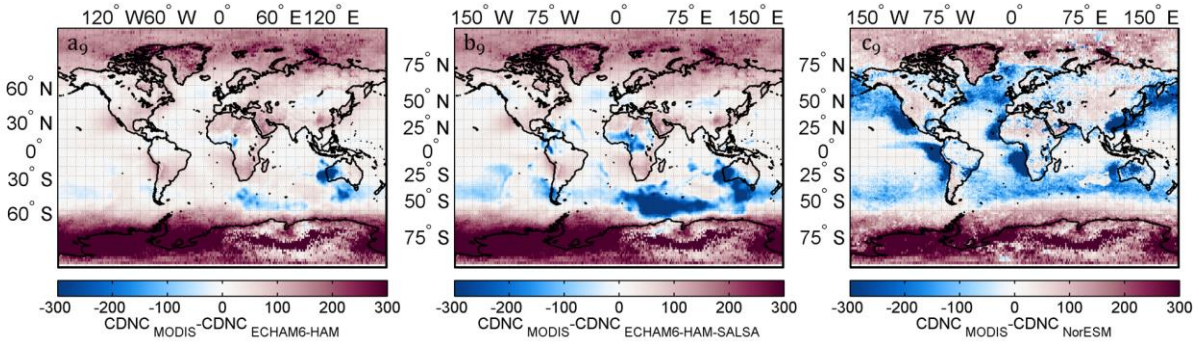
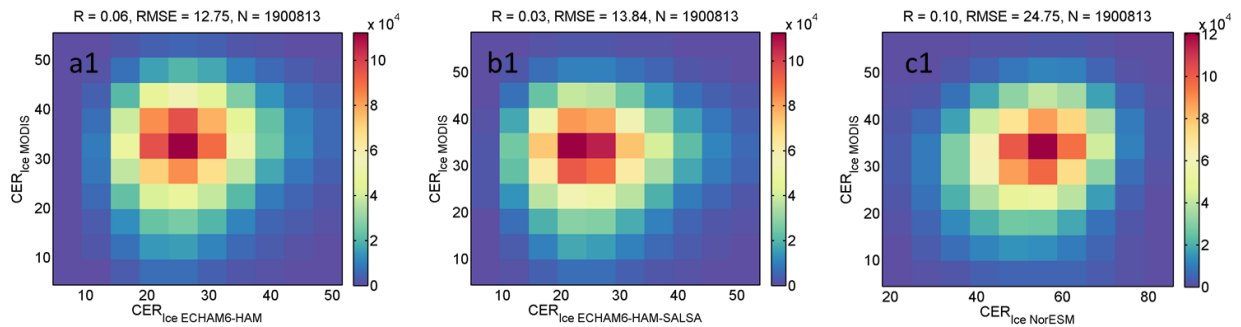
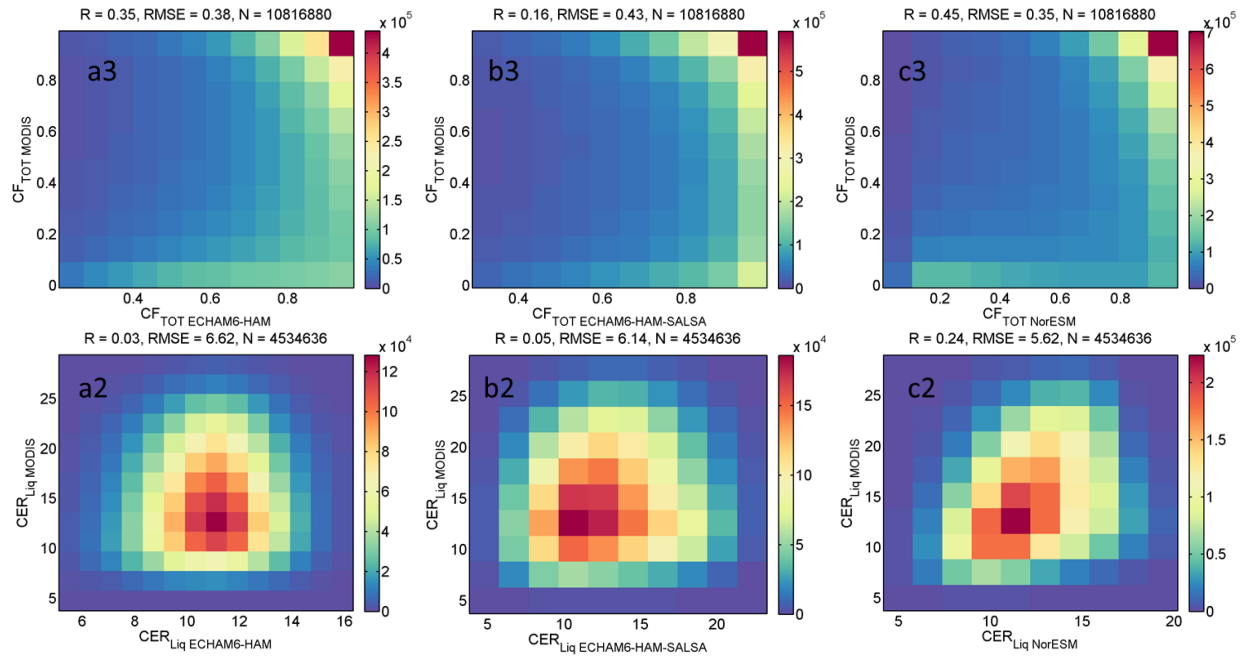


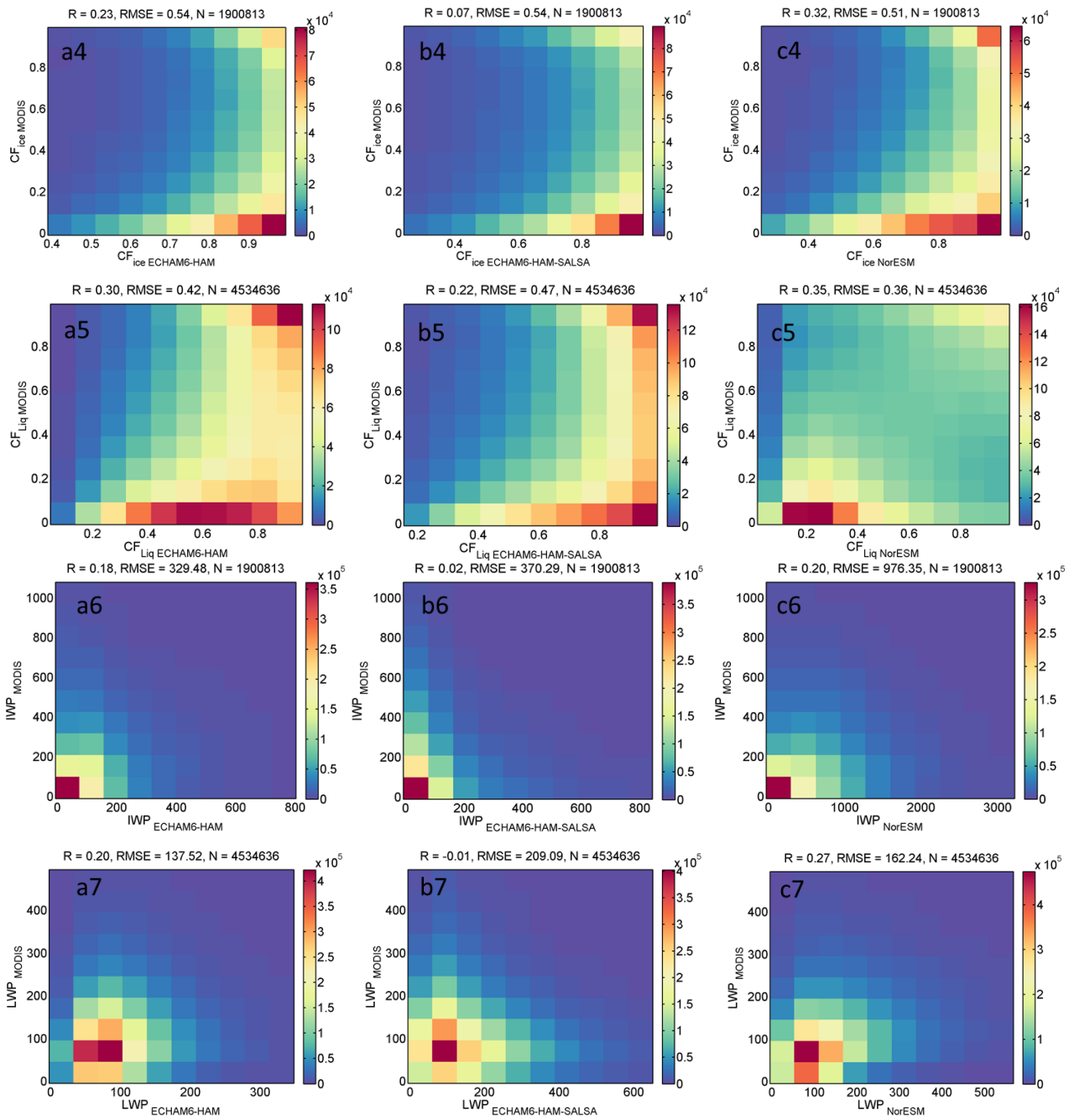
Figure 13. Spatial distribution of the difference between MODIS and ECHAM6-HAM (a), ECHAM6-HAM-SALSA (b), and NorESM(c) for CER for ice clouds (row 1) and liquid water clouds (row 2), CF for ice clouds (row 3), liquid clouds (row 4), and total CF (row 5), IWP (row 6), LWP (row 7), AOD (row 8), CDNC (row 9).

2D histogram plots

The 2D histogram plots for each parameter are shown in Fig.5. The number of bins used to derive the plots is calculated by using Scott's normal reference rule (Scott, 2010). As the datasets are collocated, the number of points is the same for each parameter.







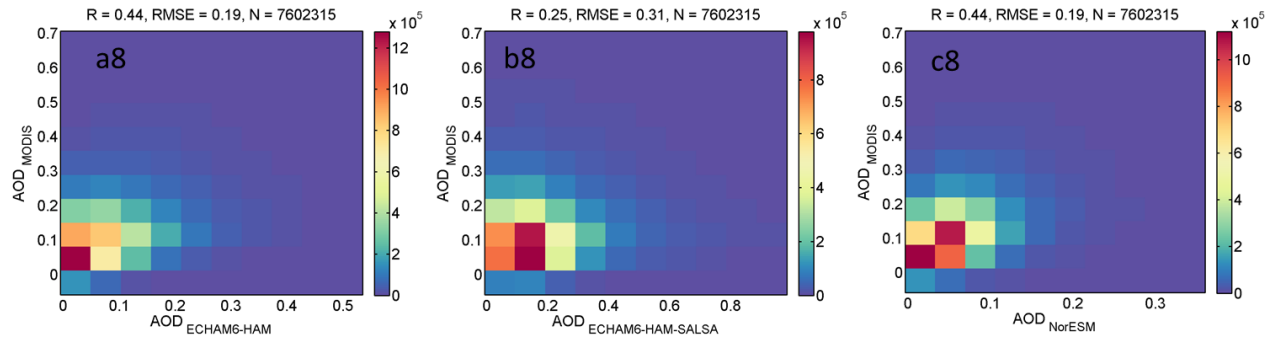


Figure 14. Density plots of MODIS and ECHAM6-HAM (a), ECHAM6-HAM-SALSA (b), and NorESM(c) for CER for ice clouds (row 1) and liquid water clouds (row 2), total CF (row 3), CF for ice clouds (row 4) and liquid clouds (row 5), IWP (row 6), LWP (row7), and AOD (row 8). The correlation coefficient (R), root mean square error (RMSE) and total number of observations (N) are shown in each figure.

While the frequency distributions and spatial distributions show some agreement between the models and MODIS, these density plots show very low or no correlations between the collocated variables. Although the model simulations are nudged towards observed meteorology, there likely remains internal variability which may explain part of the low correlations.

One way to understand why this is the case is to look at different cloud types by creating joint histograms relating cloud top pressure, cloud optical thickness and cloud fraction. These are available from MODIS and COSP-based MODIS retrievals from ECHAM6-HAM and ECHAM6-HAM-SALSA as well for NorESM, although the latter has different bin boundaries. The results are shown in Fig.15: although differences are seen across the entire ranges, patterns are similar between ECHAM6-HAM and ECHAM6-HAM-SALSA, and MODIS and NorESM. MODIS, ECHAM6-HAM and ECHAM6-HAM-SALSA do not detect very optically thin clouds ($COT < 0.3$), while small fraction of data are provided for $CTP > 620\text{hPa}$ by NorESM (Fig. 15d). Optically thin clouds ($0.3 < COT < 1.3$) are detected by MODIS only at $CTP < 680\text{hPa}$ while ECHAM6-HAM and ECHAM6-HAM-SALSA provides values only for $CTP > 680\text{hPa}$. All four dataset show a good agreement for middle-low altitudes ($CTP > 680\text{hPa}$ for ECHAM6-HAM and ECHAM6-HAM-SALSA and MODIS, 620hPa for NorESM) and optically thin clouds ($3.6 < COT < 23$). Unlike ECHAM6-HAM and ECHAM6-HAM-SALSA, MODIS and NorESM shows higher percentage of data at high altitudes.

ECHAM6-HAM underestimates CER_{liq} (Fig.4, Fig. 7, Fig. 13a1, and Fig. 14a2) compared to MODIS while ECHAM6-HAM-SALSA overestimates LWP (Fig. 13b7, Fig. 14b7) compared to MODIS.

COT of low altitude clouds seems higher for ECHAM6-HAM and ECHAM6-HAM-SALSA than for MODIS. This is likely due to the underestimation of CER_{liq} in ECHAM6-HAM and overestimation of LWP in ECHAM6-HAM-SALSA. CF_{liq} on the other hand is underestimated in ECHAM6-HAM and ECHAM6-HAM-SALSA compared to MODIS (Fig. 13a4 and b4). This is consistent with the evaluation by Stevens et al. (2013) for ECHAM6 where biases for marine boundary layer clouds were found: “too few, too bright”.

COT and frequency of high altitude clouds on the other hand are lower in ECHAM6-HAM and ECHAM6-HAM-SALSA than for MODIS. An underestimation of CF_{ice} can be seen in Fig. 13 a3, b3 and c3 for all the models compared to MODIS. Why COT of high/ice clouds is underestimated in ECHAM6-HAM and ECHAM6-HAM-SALSA is unclear as both models show some agreement of CER_{ice} and IWP compared with MODIS (Fig. 4, 6, 11, 13a2, b2, a4, b6).

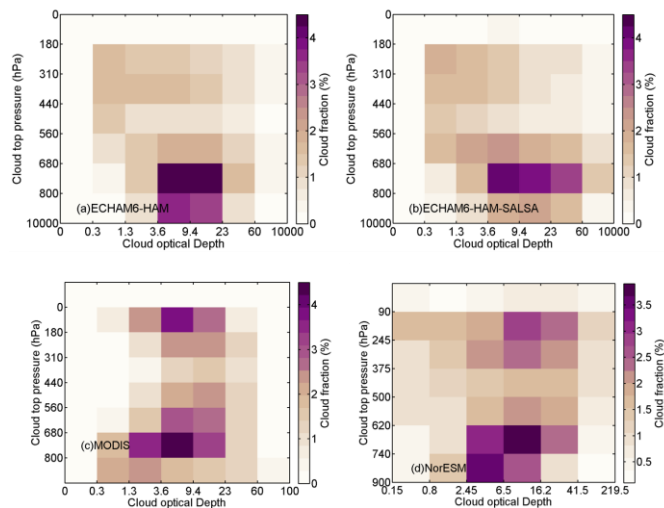


Figure 15. Global mean cloud fraction as a function of cloud top pressure (y-axis) and cloud optical depth (x-axis) from ECHAM6-HAM (a), ECHAM6-HAM-SALSA (b), MODIS (c) and NorESM (d)

Relationship between AOD and cloud parameters

The relationship between the observed cloud parameter with MODIS AOD shown in Fig. 16 is a way to observe the cloud response to aerosols. AOD values above 1 are not included because of the negligible amount of data in this range of values. Each bin has to have at least 50 counts.

Global

Nonetheless the cloud fraction from NorESM and MODIS shows always a significant increase with AOD, especially for AOD below 0.2, while the other two models seem to be not affected (Fig.16 a-c), Quaas et al. (2010) has shown that CF-AOD relationship is affected by covariation of humidity.

In the case of CER for liquid-water clouds (Fig.16e), all data sources present a very strong decrease for $AOD < 0.6$. MODIS CER inversed relationship with AOD is not so accentuated and levels off for $AOD > 0.2$. Figure 16c show how higher the estimates of CF for ice clouds from NorESM are compared to the remaining datasets. Modest changes of LWP (Fig.16g) are illustrated for MODIS and NorESM, where beside the large bias the functions have the same trend, while the other two models slightly increase as a function of AOD. The LWP for all the models (Fig1.6g) significantly increases with AOD, but, in contrast, MODIS LWP is rather constant. IWP (Fig.16g) show a constant trend of the modelling and MODIS values.

Regional scale

The results for different geographical regions (Appendix A) does not present significant discrepancies with corresponding analysis on a global scale.

The previous sections showed the large discrepancies between MODIS and modeling data. These findings suggest the need to constrain each model parametrization to better fit the relationship with MODIS data. The work is on-going.

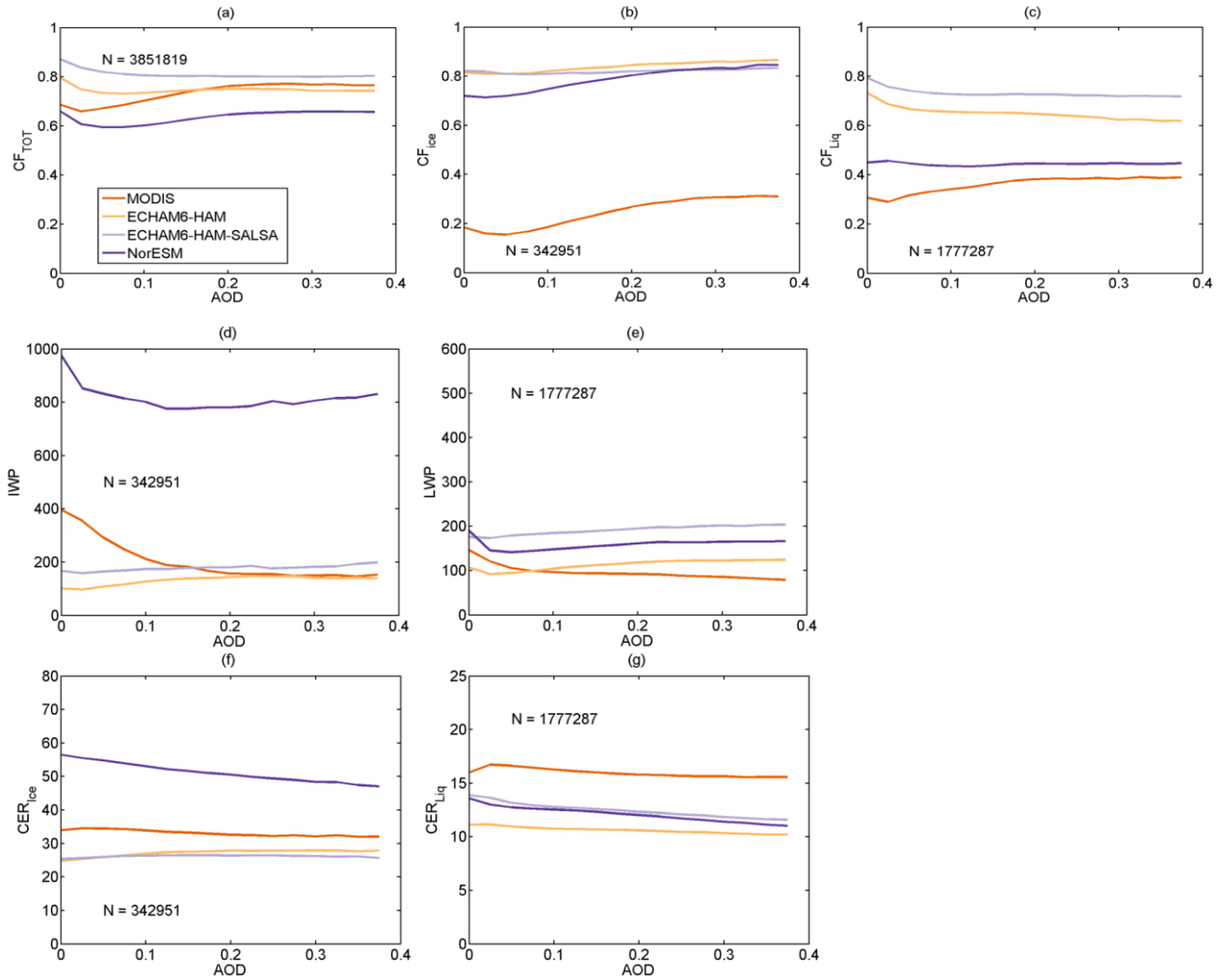


Figure 16. CF for total (a), ice (b) and liquid (c) clouds, IWP (d) and LWP (e), CER for ice clouds (f) and liquid water clouds (g), as a function AOD.

4.1. Regional case study – Amazon

With the aim of associating parameters from different satellite datasets, cloud optical properties at 1km x 1km resolution from the MODIS and ADV algorithm are directly compared. The chosen satellite instruments for the tasks were MODIS and AATSR as they both have well validated aerosol products together with cloud products with multiple cloud parameters.

The retrieved aerosol property considered here is the aerosol optical depth. Other retrieved aerosol parameters, such as the Ångström exponent and the single scattering albedo providing additional information about the size distribution and absorption properties of aerosol particles, are currently rather experimental and do not have reliable validation results over land and ocean.

We use Level 2 MODIS- and ADV/ASV-retrieved aerosol and cloud properties over an extended area of the Amazon that includes also the Caribbean. As ENVISAT was lost in 2012, the ADV/ASV algorithm designed for processing AATSR data is constrained by this temporal limit. The focus is on liquid clouds.

The standard MODIS aerosol Level 2 product, MxD04, has a $10 \times 10 \text{ km}^2$ resolution. The ADV/ASV algorithm retrieves aerosol properties at $10 \times 10 \text{ km}^2$. These aerosol parameters are collocated in time and space to derive spatial distribution over the case study area as well as compared, locally, with the AERONET stations showed in Fig.17.

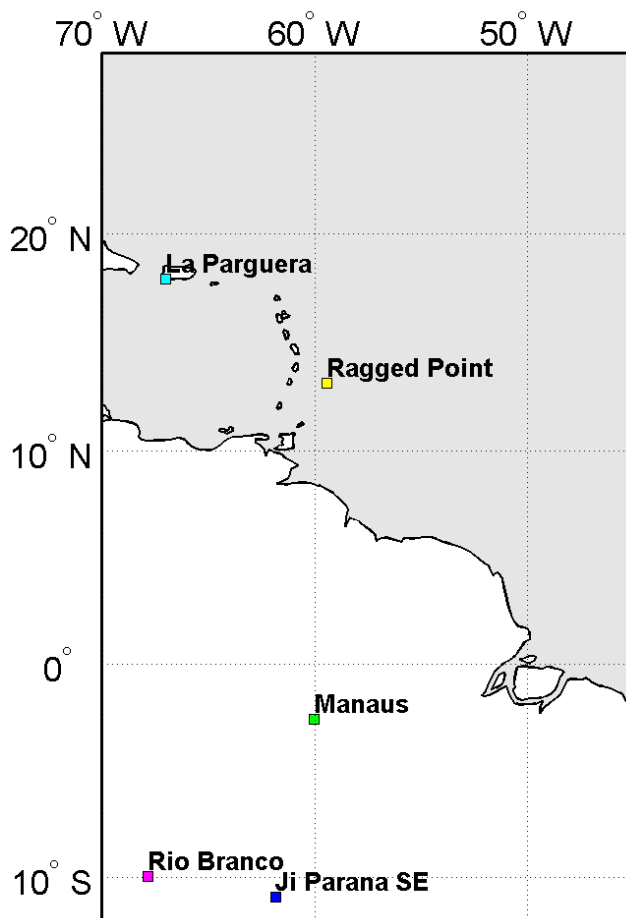


Figure 17. Map of the Aeronet stations used for the AOD comparison with MODIS and AATSR data.

The scatter plots (Fig.18, Fig.19) shows that overall the AOD derived from AATSR is overestimating, resulting in slightly lower correlation coefficients for each AERONET case when compared with MODIS results. In particular very large estimates are over the station of Ragged Point. One possible explanation is that ADV/ASV fails retrieving over the shallow waters around this station. Moreover, fewer matches between AATSR and AERONET are available because the ADV global coverage is 5-6 days instead of the 1-2 days coverage provided by MODIS.

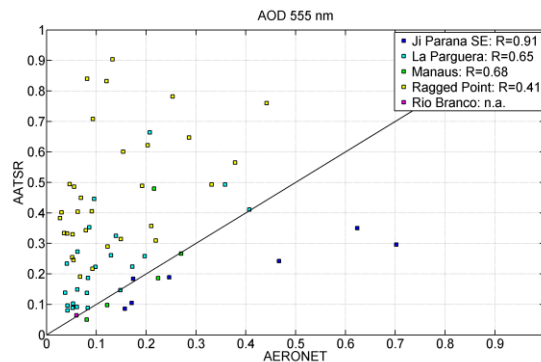


Figure 18. Scatter plot of ADV/ASV AATSR data and AERONET. The points are color-coded representing the different AERONET stations. The correlation coefficient for each comparison is presented in the legend, next to the name of the AERONET stations.

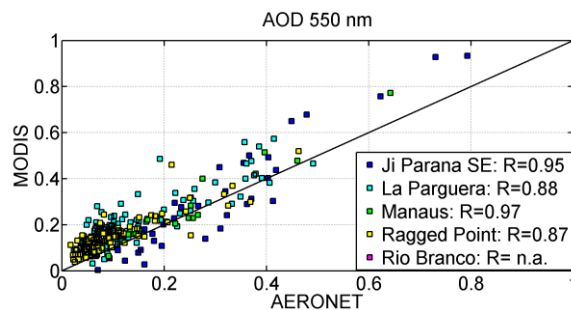


Figure 19. Scatter plot of MODIS data and AERONET. The points are color-coded representing the different AERONET stations. The correlation coefficient for each comparison is presented in the legend, next to the name of the AERONET stations.

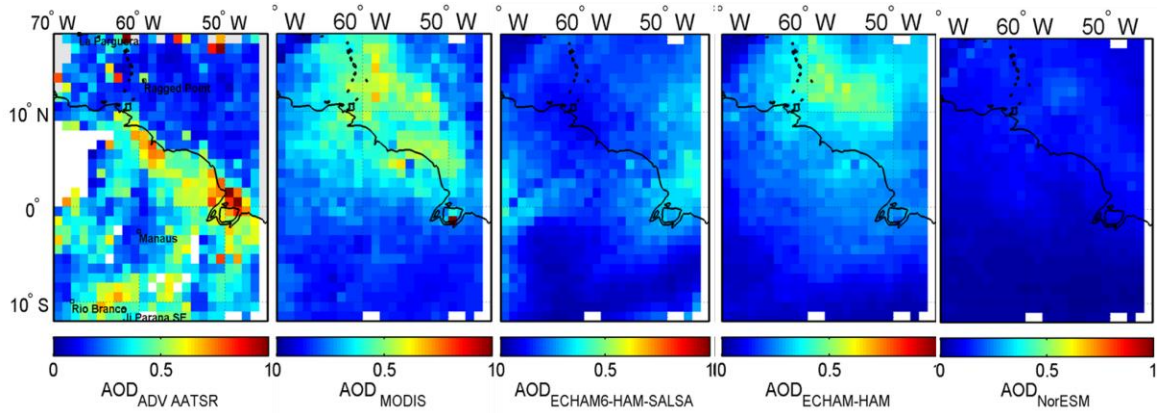


Figure 20. Comparison of spatial distribution of AOD for liquid clouds obtained from, starting from the left, AATSR, MODIS, ECHAM6-HAM-SALSA, ECHAM6-HAM and NorESM.

To compare the different data sources, aerosol and cloud optical properties at 1x1 degree grid resolution from ECHAM6-HAM, ECHAM6-HAM-SALSA, MODIS, NorESM and ADV/ASV retrievals were directly compared (Fig. 20, Fig.21). The focus is on liquid clouds. These parameters are collocated in time and space to derive spatial distributions of the aerosol cloud properties over the Amazon case study during October 2008. Considering that the data is from one month only, the spatial distributions of AOD and CER (Fig.20 and Fig.21) show large disagreements between the five data sources.

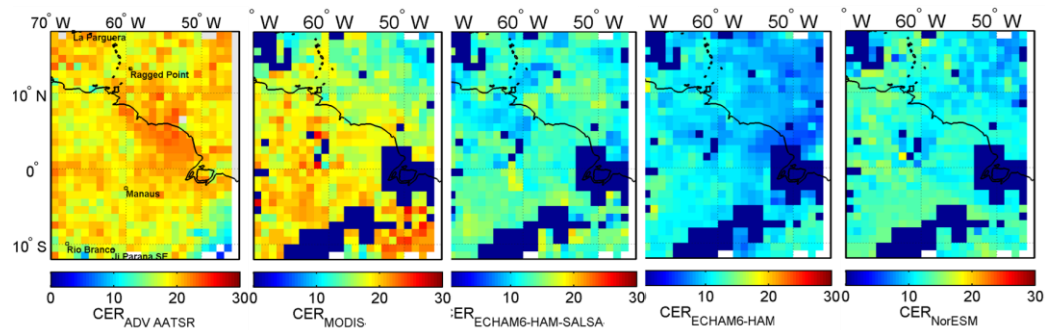


Figure 21. Comparison of spatial distribution of CER for liquid clouds obtained from, starting from the left, SACURA AATSR, MODIS, ECHAM6-HAM-SALSA, ECHAM6-HAM and NorESM.

Changes with respect to the DoW

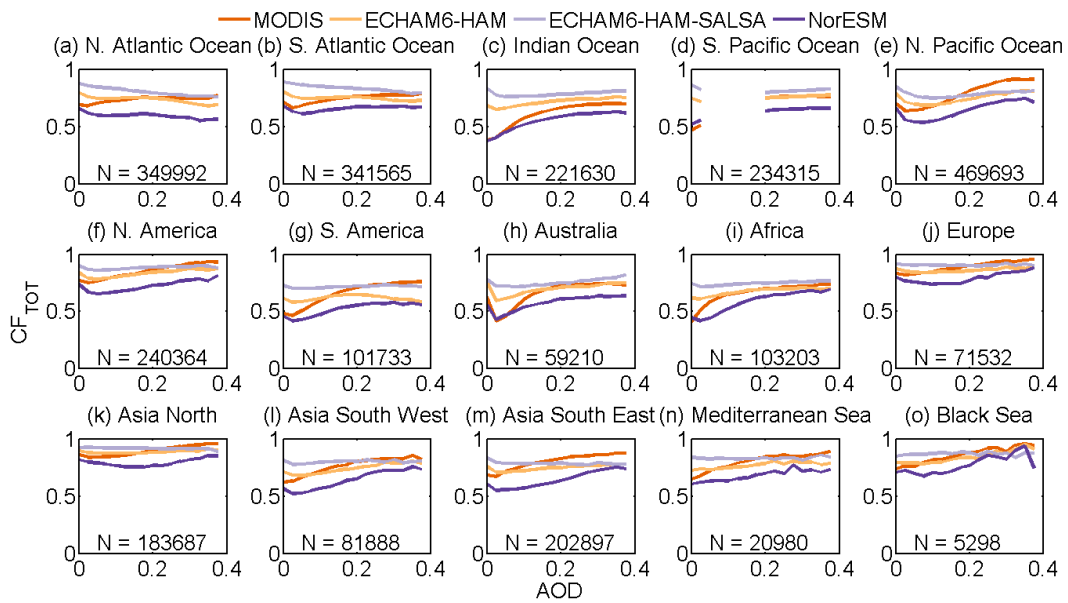
None

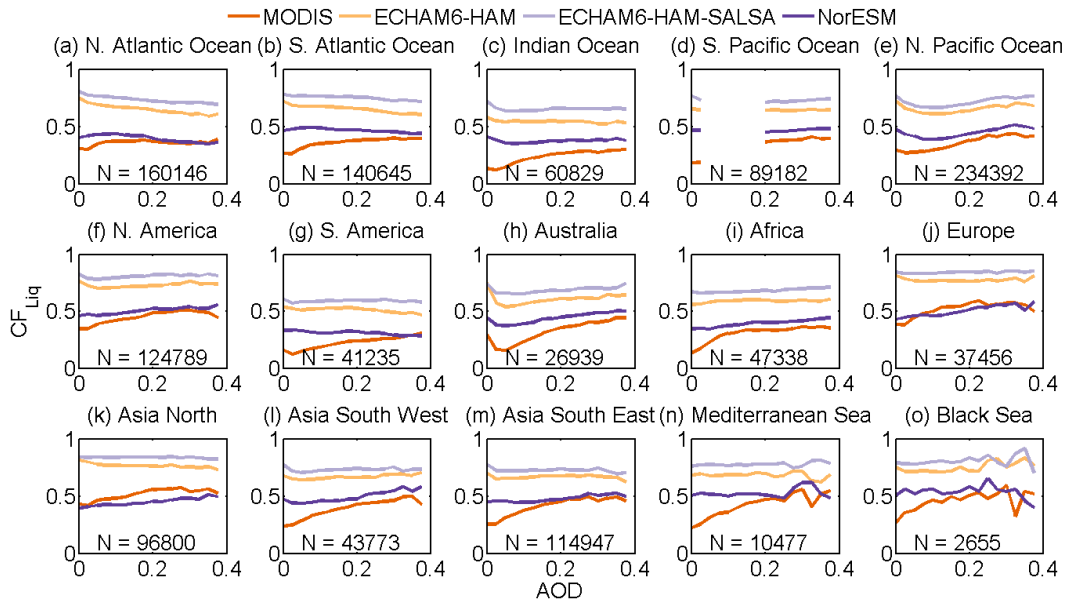
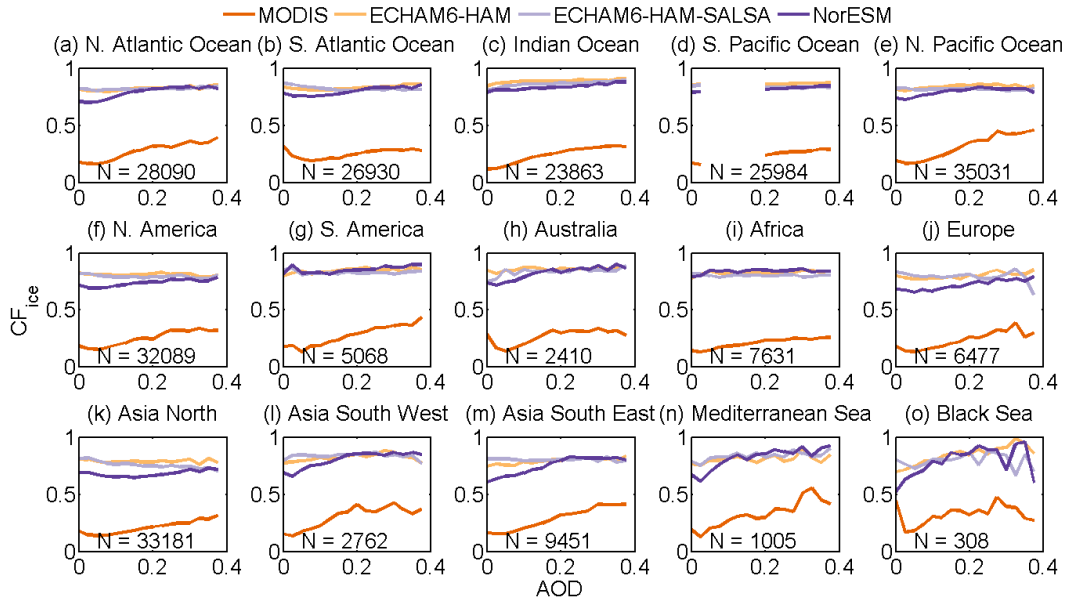
Dissemination and uptake

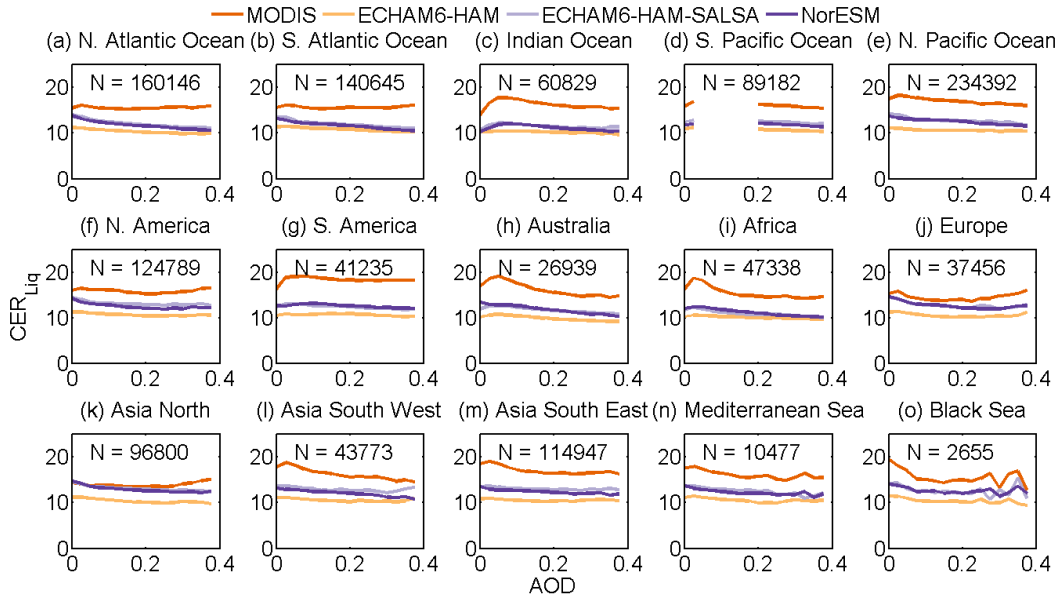
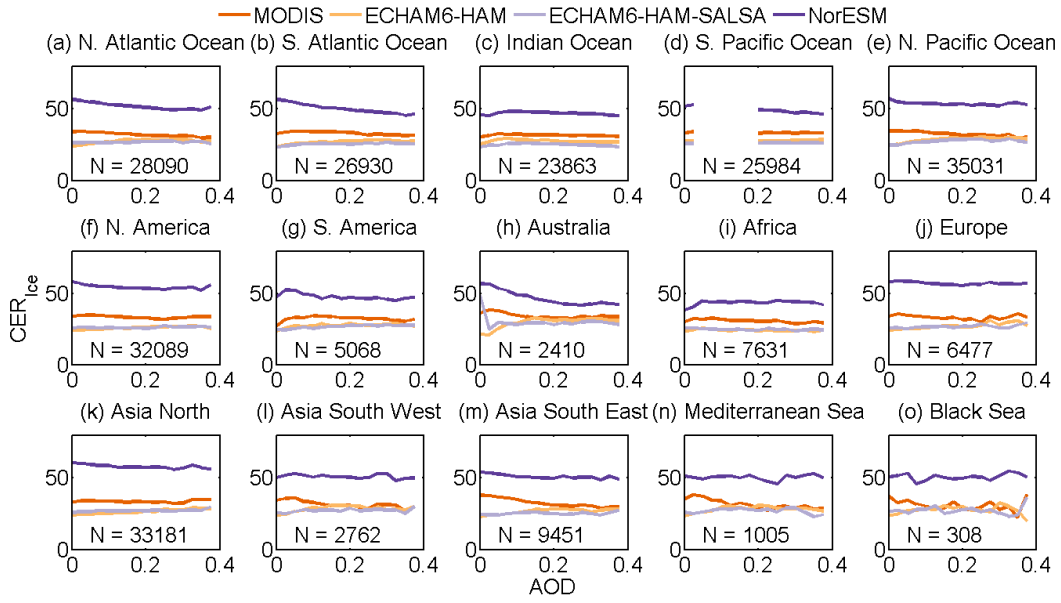
The deliverable is useful for both the modeling and satellite community interested in applying COSP 1.4 for satellite and ESM comparison

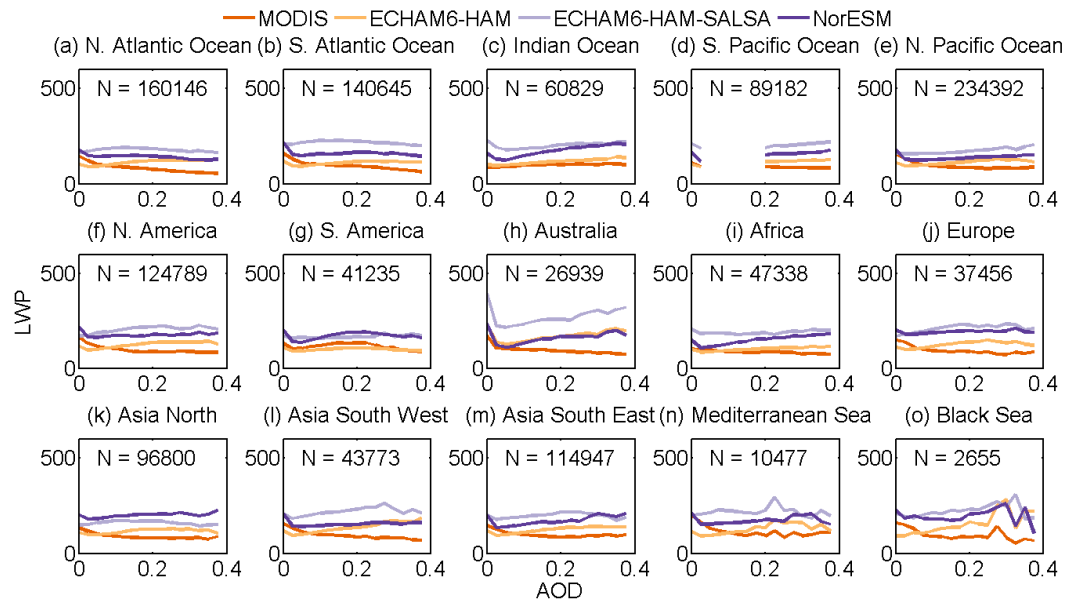
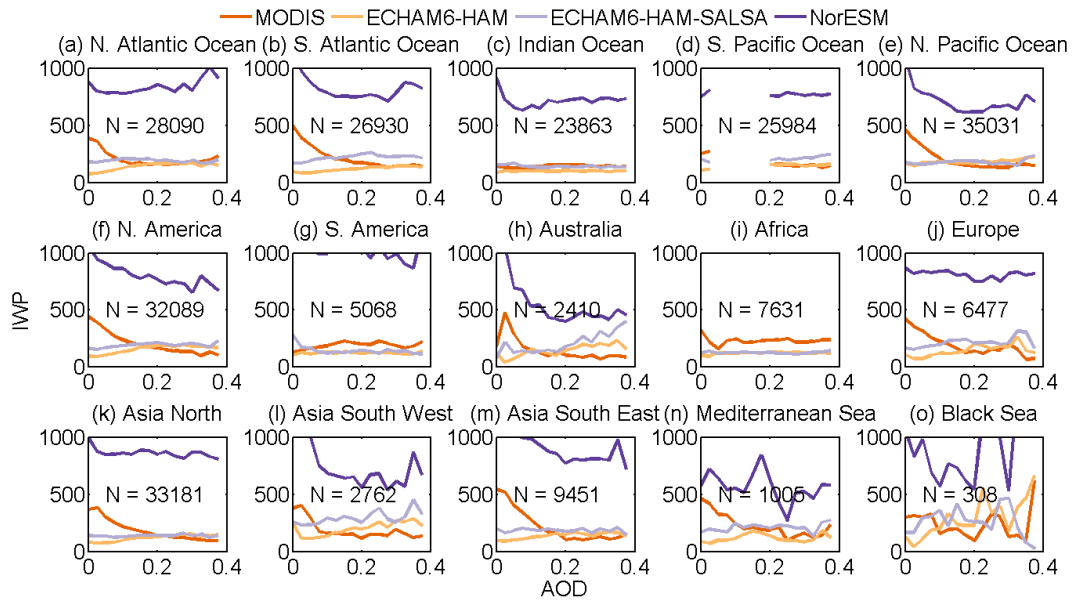
5. Appendixes

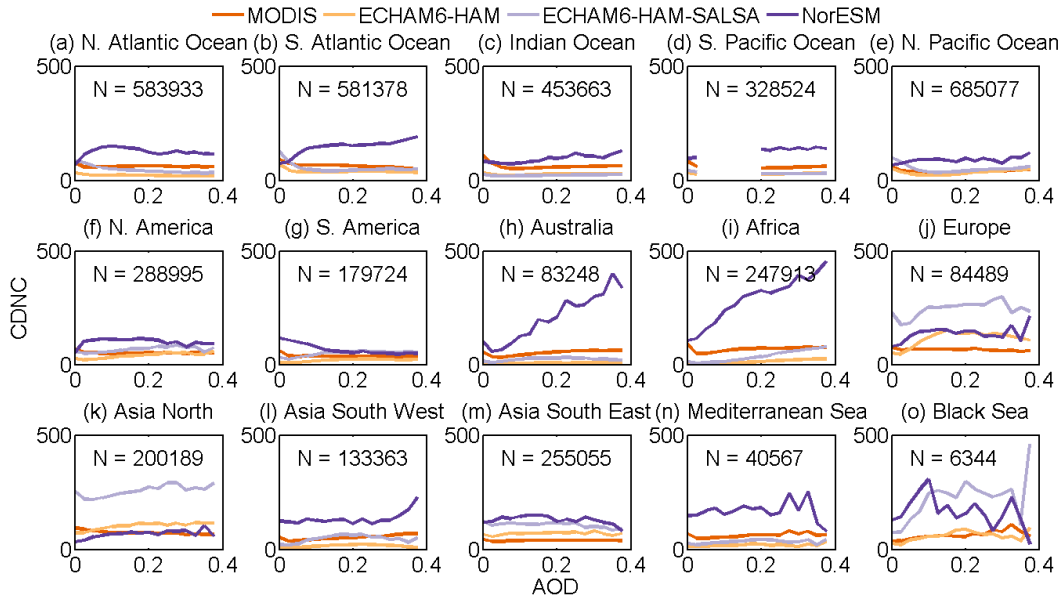
Appendix A











Appendix B

Table 1. List of the parameters available from ECHAM6-HAM, ECHAM6-HAM-SALSA, NorESM, and MODIS

Variable name	Units	COSP /direct	Dimensi on	ECHAM6-HAM-SALSA	ECHAM6-HAM	NorESM	MODIS
AI	-	Direct	2d	yes	yes	yes	yes
AOD	-	Direct	2d	yes	yes	yes	yes
AOD clear sky	-	Direct	2d	no	no	yes	no
CDNC	m ³	Direct	3d	yes	yes	yes (AWNC)	yes
CLDEMISS	-	Direct	3d	yes	yes	no	yes
CLIMODIS	%	COSP	2d	yes	yes	yes	yes
CF	%	Direct	3d	yes	yes	yes	-
CF hist	%	COSP	2d	yes (histmodis)	yes (histmodis)	yes	yes

CLTMODIS	%	COSP	2d	yes	yes	yes	yes
CLWMODIS	%	COSP	2d	yes	yes	yes	yes
CRELW	W/m2	Direct	2d	no	yes	yes (LWCF)	-
CRENET	W/m2	Direct	2d	no	yes	yes (FLNT)	-
CRESW	W/m2	Direct	2d	no	yes	yes (SWCF)	-
FLWTOA	W/m2	Direct	2d	no	yes	yes	-
FSWTOA	W/m2	Direct	2d	no	yes	yes	-
GEOP_LEV	m2/s2	Direct	3d	yes	yes	no	-
GEOP_SUR F	m2/s2	Direct	3d	yes	yes	yes	-
ICNC	m3	Direct	3d	yes	yes	yes (AWNI)	yes
IWC	kg/kg _air	Direct	3d	yes	yes	yes	-
IWPMODIS	kg/m2	COSP	2d	yes	yes	yes	yes
IWP	kg/m2	Direct	2d	yes	yes	yes	-
LWPMODIS	kg/m2	COSP	2d	yes	yes	yes	yes
LWP	kg/m2	Direct	2d	yes	yes	yes	-
Tb IR ISCCP	K	COSP	2d	no	no	yes (MEANT B_ISCCP)	-
PSURF	Pa	Direct	2d	yes	yes	yes	-
REFFLCLI MODIS	m	COSP	2d	yes	yes	yes	yes
REFFLCLW MODIS	m	COSP	2d	yes	yes	yes	yes
REFFI	um	Direct	3d	yes	yes	yes	-

						(AREI)	
REFFL	um	Direct	3d	yes	yes	yes (AREL)	-
TCC	%	Direct	2d	yes	yes	yes	yes
T	K	direct	3d	yes	yes	yes	-

Table 2. List of acronyms and their definition.

Acronym	Definition
AI	aerosol index
AOD	aerosol optical depth all sky condition
AOD clear sky	aerosol optical depth in clear sky condition
CDNC	cloud droplet number concentration
CLDEMISS	cloud emissivity
CLIMODIS	total ice cloud amount
CF	cloud fraction
CF MODIS	cloud fraction from MODIS-COSP
CLTMODIS	cloud total amount
CLWMODIS	total liquid water amount
CRELW	cloud radiative effect at long wavelengths
CRENET	net cloud radiative effect
CRESW	cloud radiative effect at short wavelengths
FLWTOA	Longwave Forcing at the top of the atmosphere
FSWTOA	Shortwave Forcing at the top of the atmosphere
GEOP_LEV	geopotential at model level
GEOP_SURF	geopotential of surface
ICNC	ice crystal number concentration
IWC	ice water content
IWPMODIS	ice water content from MODIS-COSP
IWP	ice water path

LWPMODIS	liquid water path from MODIS-COSP
LWP	liquid water path
Tb IR ISCCP	Mean Infrared Tb from ISCCP simulator
PSURF	surface pressure
REFFLCLIMODIS	cloud effective radius for ice clouds from MODIS-COSP
REFFLCLWMODIS	cloud effective radius for liquid clouds from MODIS-COSP
REFFI	cloud effective radius for ice clouds
REFFL	cloud effective radius for liquid clouds
TCC	total cloud cover
T	temperature

6. References

Bentsen, M., Bethke, I., Debernard, J., Iversen, T., Kirkevåg, A., Seland, Ø., Drange, H., Roelandt, C., Seierstad, I., and Hoose, C.: The Norwegian earth system model, NorESM1-M—Part 1: description and basic evaluation of the physical climate, *Geosci. Model Dev*, 6, 687-720, 2013.

Bergman, T., Kerminen, V.-M., Korhonen, H., Lehtinen, K. J., Makkonen, R., Arola, A., Mielonen, T., Romakkaniemi, S., Kulmala, M., and Kokkola, H.: Evaluation of the sectional aerosol microphysics module SALSA implementation in ECHAM5-HAM aerosol-climate model, *Geosci. Model Dev.*, 5, 845-868, doi:10.5194/gmd-5-845-2012, 2012.

Berrisford, P., Kallberg, P., Kobayashi, S., Dee, D., Uppala, S., Simmons, A. J., Poli, P., and Sato, H.: Atmospheric conservation properties in ERA-Interim, *Q J Roy Meteor Soc*, 137, 1381-1399, 10.1002/qj.864, 2011.

Brenguier, J. L., Pawlowska, H., Schuller, L., Preusker, R., Fischer, J., and Fouquart, Y.: Radiative properties of boundary layer clouds: Droplet effective radius versus number concentration, *J. Atmos. Sci.*, 57, 803-821, 2000.

Dee, D. P., Uppala, S. M., Simmons, A. J., Berrisford, P., Poli, P., Kobayashi, S., Andrae, U., Balmaseda, M. A., Balsamo, G., Bauer, P., Bechtold, P., Beljaars, A. C. M., van de Berg, L., Bidlot, J., Bormann, N., Delsol, C., Dragani, R., Fuentes, M., Geer, A. J., Haimberger, L., Healy, S. B., Hersbach, H., Holm, E. V., Isaksen, L., Kallberg, P., Kohler, M., Matricardi, M., McNally, A. P., Monge-Sanz, B. M., Morcrette, J.-J., Park, B.-K., Peubey, C., de

Rosnay, P., Tavolato, C., Thépaut, J.-N., and Vitart, F.: The ERA-Interim reanalysis: configuration and performance of the data assimilation system, *Q. J. Roy. Meteor. Soc.*, 137, 553–597, 10.1002/qj.828, 10.1002/qj.828, 2011.

Gottelman, A., and Morrison, H.: Advanced Two-Moment Bulk Microphysics for Global Models. Part I: Off-Line Tests and Comparison with Other Schemes, *J Climate*, 28, 1268-1287, 10.1175/Jcli-D-14-00102.1, 2015.

Ghan, S. J., and Easter, R. C.: Impact of cloud-borne aerosol representation on aerosol direct and indirect effects, *Atmos Chem Phys*, 6, 4163-4174, 2006.

Guenther, A. B., Jiang, X., Heald, C. L., Sakulyanontvittaya, T., Duhl, T., Emmons, L. K., and Wang, X.: The Model of Emissions of Gases and Aerosols from Nature version 2.1 (MEGAN2.1): an extended and updated framework for modeling biogenic emissions, *Geosci Model Dev*, 5, 1471-1492, 10.5194/gmd-5-1471-2012, 2012.

Grandey, B. S., Stier, P., and Wagner, T. M.: Investigating relationships between aerosol optical depth and cloud fraction using satellite, aerosol reanalysis and general circulation model data, *Atmos. Chem. Phys.*, 13, 3177-3184, doi:10.5194/acp-13-3177-2013, 2013.

Hubanks, P. A., Platnick, S., King, M. D., and Ridgway, B.: MODIS Atmosphere L3 Gridded Product Algorithm Theoretical Basis Document (ATBD) & Users Guide, Collection 006, Version 4.2., NASA-GSFC, 122, 2016.

Karcher, B., and U. Lohmann: A Parameterization of cirrus cloud formation: Homogeneous freezing including effects of aerosol size, *J. Geophys. Res.*, 107 (D23), 4698, doi:10.1029/2001JD001429, 2002.

Khairoutdinov, M., and Kogan, Y.: A new cloud physics parameterization in a large-eddy simulation model of marine stratocumulus, *Mon Weather Rev*, 128, 229-243, Doi 10.1175/1520-0493(2000)128<0229:Ancppi>2.0.Co;2, 2000.

Kirkevåg, A., Grini, A., Seland, Ø., Olivie, D., Iversen, T., Schulz, M., Hummel, M., Alterskjær, K., Karset, I. H., and Lewinschal, A.: A production-tagged module for aerosols in earth system model simulations - extensions and updates for CAM5.3-Oslo, Manuscript in preparation, 2017.

Kirkevåg, A., Iversen, T., Seland, O., Hoose, C., Kristjansson, J. E., Struthers, H., Ekman, A. M. L., Ghan, S., Griesfeller, J., Nilsson, E. D., and Schulz, M.: Aerosol-climate interactions in the Norwegian Earth System Model-NorESM1-M, *Geosci Model Dev*, 6, 207-244, 10.5194/gmd-6-207-2013, 2013.

Kokkola, H., Korhonen, H., Lehtinen, K. E. J., Makkonen, R., Asmi, A., Järvenoja, S., Anttila, T., Partanen, A.-I., Kulmala, M., Järvinen, H., Laaksonen, A., and Kerminen, V.-M.: SALSA – a Sectional Aerosol module for Large Scale Applications, *Atmos. Chem. Phys.*, 8, 2469-2483, doi:10.5194/acp-8-2469-2008, 2008.

Kolmonen, P., Sogacheva, L., Virtanen, T. H., de Leeuw, G., and Kulmala, M.: The ADV/ASV AATSR aerosol retrieval algorithm: current status and presentation of a full-mission AOD dataset, *International Journal of Digital Earth*, 9:6, 545-561 (2016), DOI: 10.1080/17538947.2015.1111450.

Laakso, A., Kokkola, H., Partanen, A.-I., Niemeier, U., Timmreck, C., Lehtinen, K. E. J., Hakkarainen, H., and Korhonen, H.: Radiative and climate impacts of a large volcanic eruption during stratospheric sulfur geoengineering, *Atmos. Chem. Phys.*, 16, 305-323, doi:10.5194/acp-16-305-2016, 2016.

Levy, R. C., Mattoo, S., Munchak, L. A., Remer, L. A., Sayer, A.M., Patadia, F., and Hsu, N. C.: The Collection 6 MODIS aerosol products over land and ocean, *Atmos. Meas. Tech.*, 6, 2989–3034, doi:10.5194/amt-6-2989-2013, 2013

Liu, X., Easter, R. C., Ghan, S. J., Zaveri, R., Rasch, P., Shi, X., Lamarque, J. F., Gettelman, A., Morrison, H., Vitt, F., Conley, A., Park, S., Neale, R., Hannay, C., Ekman, A. M. L., Hess, P., Mahowald, N., Collins, W., Iacono, M. J., Bretherton, C. S., Flanner, M. G., and Mitchell, D.: Toward a minimal representation of aerosols in climate models: description and evaluation in the Community Atmosphere Model CAM5, *Geosci Model Dev*, 5, 709-739, 10.5194/gmd-5-709-2012, 2012.

Lohmann, U., and K. Diehl (2006), Sensitivity studies of the importance of dust ice nuclei for the indirect aerosol effect on stratiform mixed phase clouds, *J. Atmos. Sci.*, 63, 968-982.

Lohmann, U., and C. Hoose (2009), Sensitivity studies of different aerosol indirect effects in mixed-phase clouds, *Atmos. Chem. Phys.*, 9, 8917-8934, doi:10.5194/acp-9-8917-2009.

Lohmann, U. and E. Roeckner (1996), Design and performance of a new cloud microphysics scheme developed for the ECHAM general circulation model, *Clim. Dyn.*, 12, 557-572.

Lohmann, U., P. Spichtinger, S. Jess, T. Peter, and H. Smit (2008), Cirrus cloud formation and ice supersaturated regions in a global climate model, *Env. Res. Lett.*, 3, 045022.

Myhre, G., Stordal, F., Johnsrud, M., Kaufman, Y.J., Rosenfeld, D., Storelvmo, T., Kristjansson, J.E., Berntsen, T.K., Myhre, A., and Isaksen, I.S.A: Aerosol-cloud interaction inferred from MODIS satellite data and global aerosol models, *Atmos. Chem. Phys.*, 7, 3081-3101, 2007.

Morrison, H., and Gettelman, A.: A new two-moment bulk stratiform cloud microphysics scheme in the community atmosphere model, version 3 (CAM3). Part I: Description and numerical tests, *J Climate*, 21, 3642-3659, 10.1175/2008jcli2105.1, 2008.

Oleson, K. W., Lawrence, D. M., Gordon, B., Flanner, M. G., Kluzek, E., Peter, J., Levis, S., Swenson, S. C., Thornton, E., and Feddema, J.: Technical description of version 4.0 of the Community Land Model (CLM), 2010.

Park, S., and Bretherton, C. S.: The University of Washington Shallow Convection and Moist Turbulence Schemes and Their Impact on Climate Simulations with the Community Atmosphere Model, *J Climate*, 22, 3449-3469, 10.1175/2008jcli2557.1, 2009.

Quaas, J., Stevens, B., Stier, P., and Lohmann, U.: Interpreting the cloud cover – aerosol optical depth relationship found in satellite data using a general circulation model, *Atmos. Chem. Phys.*, 10, 6129-6135, doi:10.5194/acp-10-6129-2010, 2010.

Sogacheva, L., Kolmonen, P., Virtanen, T. H., Rodriguez, E., Saponaro, G. and de Leeuw, G.: Post-processing to remove residual clouds from aerosol optical depth retrieved using the Advanced Along Track Scanning Radiometer, *Atmos. Meas. Tech.*, 10, 491-505 (2017).

Scott, D. W.: Scott's rule, *WIREs Comp Stat*, 2: 497–502. doi:10.1002/wics.103, 2010.

Stevens, B., Giorgetta, M., Esch, M., Mauritsen, T., Crueger, T., Rast, S., Salzmann, M., Schmidt, H., Bader, J., Block, K., Brokopf, R., Fast, I., Kinne, S., Kornbluh, L., Lohmann, U., Pincus, R., Reichler, T., and Roeckner, E.: Atmospheric component of the MPI-M Earth System Model: ECHAM6, *J. Adv. Model. Earth Syst.*, 5, 146–172, doi:10.1002/jame.20015, 2013.

Wang, Y., Liu, X., Hoose, C., and Wang, B.: Different contact angle distributions for heterogeneous ice nucleation in the Community Atmospheric Model version 5, *Atmos Chem Phys*, 14, 10411-10430, 10.5194/acp-14-10411-2014, 2014.

Zhang, G., and McFarlane, N. A.: Sensitivity of climate simulations to the parameterization of cumulus convection in the Canadian Climate Centre general circulation model, *Atmosphere-ocean*, 33, 407-446, 1995.

Zhang, Z., A.S. Ackerman, G. Feingold, S. Platnick, R. Pincus, and H. Xue: Effects of cloud horizontal inhomogeneity and drizzle on remote sensing of cloud droplet effective radius: Case studies based on large-eddy simulations. *J. Geophys. Res.*, 117, no. D19, D19208, doi:10.1029/2012JD017655. , 2012